Valence Structures and Electron Spin Dynamics in Halogen-Bridged One-Dimensional Metal Complexes Studied by Magnetic Resonances

Noriyoshi KIMURA

A dissertation submitted to the Doctoral Program
in Chemistry, the University of Tsukuba
in partial fulfillment of the requirements for the
degree of Doctor of Philosophy (Science)

January, 1998

Contents

Chapter 1

General Introduction

Halogen-bridged -M^{2+}-X-M^{4+}-X- type complexes (M: Pt, Pd and X: Cl, Br, I), typified by Wolffram's red salt $[Pt(C_2H_5NH_2)_4][PtCl_2(C_2H_5NH_2)_4]Cl_4 \cdot 4H_2O$, have been attracting much attention among solid-state physicists and chemists as a one-dimensional (1-D) system with strong electron-lattice interactions after the 1970's because of their remarkable physical properties such as intense intervalence charge transfer bands [1-3], luminescence with a large Stokes-shift [3,4], overtone progressions observed in resonance Raman spectra [5], *etc.* These features are common in this type of mixed-valence metal complexes consisting of various combinations of metal atoms, bridged halogens, amine ligands and counter ions.

It is noted in this type mixed valence complexes that there is a twofold degeneracy of the electronic ground state expressed as: - 2 - 4 - 2 - 4 - and - 4 - 2 - 4 - 2 - in this chain structure. From this degeneracy, we can expect the formation of the mismatch of these two structures in crystal. The boundary of these structure called the domain wall, expressed, for example, as -M^{2+}-X-M^{4+}-X-M^{3+}-X-M^{2+}-X-M^{4+}-X-, has been theoretically derived [6,7] in a similar manner to the neutral spin soliton investigated in *trans*-polyacetylene [8]. The magnetic resonance measurements such as ESR and NMR are suitable for detecting the neutral solitons because of the formation of paramagnetic

spins. Since the NMR relaxation is strongly affected by the magnetic field fluctuation made by the unpaired electrons, this mechanism becomes the main origin of the relaxation even in a low concentration of the paramagnetic species in case the contribution from molecular motions to the relaxation is not important.

More than 150 1-D halogen-bridged $-M^{2+}-X-M^{4+}-X-$ type mixed-valence complexes formulated as $[M(AA)_2][MX_2(AA)_2]Y_4$ (M^{2+}-M^{4+}: Pt^{2+}-Pt^{4+}, Pd^{2+}-Pd^{4+}, Pd^{2+}-Pt^{4+}, Ni^{2+}-Pt^{4+}, Cu^{2+}-Pt^{4+}; X: Cl, Br, I; AA: ethylenediamine (en), 1R,2R-cyclohexanediamine (chxn), *etc.*; Y: ClO_4, X, *etc.*) have been synthesized [9-11] by M. Yamashita *et al.* in the last decade. The ESR study on single crystals of $[Pt(en)_2][PtX_2(en)_2](ClO_4)_4$ has shown the presence of the paramagnetic Pt^{3+} sites whose concentration (*ca.*10^{-4} in molar ratio to the Pt^{2+} and Pt^{4+} sites) is temperature independent [12]. It is noted that the ESR linewidth is gradually reduced with increasing temperature from 100 to 300 K suggesting the progress of motional narrowing. These ESR results suggest that the kink-type domain wall solitons introduced in the 1-D chains can diffuse in this temperature region. In the present study, the ESR spectra and the ^1H NMR relaxation time are measured to investigate dynamic behaviour of paramagnetic sites formed in $[M(en)_2][MX_2(en)_2](ClO_4)_4$.

As another kind of halogen-bridged complexes, the -M-M-X-M-M-X- type 1-D complexes, $(NH_4)_4[Pt_2X(P_2O_5H_2)_4]$ and $Ni_2(CH_3CS_2)_4I$ containing metal-metal bonds have been recently prepared [13,14]. In these complexes, new properties different

from the above -M-X-M-X- type mixed-valence complexes can be expected because of the presence of metal-metal bonds which can give metal-like properties more than in the -M-X-M-X- system. In fact, $K_4[Pt_2Br(P_2O_5H_2)_4]\cdot 3H_2O$ and $Ni_2(CH_3CS_2)_4I$ have been reported to have higher electrical conductivities of *ca.* 10^{-3} [15-17] and 10^{-2} S cm^{-1} [18], respectively, than those in -M-X-M-X- system, for example, *ca.* 10^{-8}- 10^{-18} S cm^{-1} observed in $[M(en)_2][MX_2(en)_2](ClO_4)_4$ [19], at room temperature. As for possible metal valence state, the following four models of the 1-D chain structure can be proposed:

(A) - M^{2+} - M^{2+} - X - M^{3+} - M^{3+} - X -;

(B) - M^{2+} - M^{3+} - X - M^{2+} - M^{3+} - X -;

(C) - M^{2+} - M^{3+} - X - M^{3+} - M^{2+} - X -;

(D) - $M^{2.5+}$ - $M^{2.5+}$ - X -.

Valence structures in the above Pt and Ni complexes have been discussed based on the studies of X-ray diffraction [13-18], magnetic susceptibility [17,18] and electronic and vibrational spectra [20]. No consistent conclusion on the valence structure could not be derived from the respective method. In the present study, it is intended to measure ^{31}P, ^{13}C and ^{1}H NMR which can give accurate information on metal valences. The application of solid NMR technique to the investigation of metal valences has been successfully applied to -M-X-M-X- type (M: Pt, Pd, Ni) complexes, in which ^{13}C and ^{15}N CP / MAS NMR spectra were measured [21-23].

References to Chapter 1

1. P. Day, in *Low-Dimensional Cooperative Phenomena*, ed. by H.J. Keller (Plenum Press, New York, 1975), Vol. B7, p.191.
2. H.J. Keller, in *Extended Linear Chain Compounds*, ed. by J.S. Miller (Plenum Press, New York, 1982), Vol. 1, p.357.
3. H. Tanino and K. Kobayashi, *J. Phys. Soc. Jpn.*, **52**, 1446 (1983).
4. R.J.H. Clark, M.L. Franks and W.R. Trumble, *Chem. Phys. Lett.*, **41**, 287 (1976).
5. R.J.H. Clark, in *Mixed Valence Compounds*, ed. by D.E. Brown (Reidel, Dordrecht, 1982).
6. S. Ichinose, *Solid State Commun.*, **50**, 137 (1984).
7. Y. Onodera, *J. Phys. Soc. Jpn.*, **56**, 250 (1987).
8. W.P. Su, J.R. Schrieffer and A.J. Heeger, *Phys. Rev. Lett.*, **42**, 1698 (1979).
9. N. Matsumoto, M. Yamashita and S. Kida, *Bull. Chem. Soc. Jpn.*, **51**, 2334 (1978).
10. N. Matsumoto, M. Yamashita and S. Kida, *Bull. Chem. Soc. Jpn.*, **51**, 3514 (1978).
11. R.J.H. Clark, M. Kurmoo, D.N. Mountney and H. Toftlund, *J. Chem. Soc. Dalton Trans.*, 1851 (1982).
12. A. Kawamori, R. Aoki and M. Yamashita, *J. Phys.C*, **18**, 5487 (1985).
13. S. Jin, T. Ito, K. Toriumi and M. Yamashita, *Acta Crystallogr.*, **C45**, 1415 (1989).
14. C. Bellitto, G. Dessy and V. Fares, *Inorg. Chem.*, **24**, 2815 (1985).

15. C.-M. Che, F.H. Herbstein, W.P. Schaefer, R.E. Marsh and H.B. Gray, *J. Am. Chem. Soc.*, **105**, 4604 (1983).

16. R.J.H. Clark, M. Kurmoo, H.M. Dawes and M.B. Hursthouse, *Inorg. Chem.*, **25**, 409 (1986).

17. L.G. Butler, M.H. Zietlow, C.-M. Che, W.P. Schaefer, S. Sridhar, P.J. Grunthaner, B.I. Swanson, R.J.H. Clark and H.B. Gray, *J. Am. Chem. Soc.*, **110**, 1155 (1988).

18. M. Yamashita, Y. Wada, K. Toriumi and T. Mitani, *Mol. Cryst. Liq. Cryst.*, **216**, 207 (1992).

19. Y. Hamaue, R. Aoki, M. Yamashita and S. Kida, *Inorg. Chim. Acta*, **54**, L13 (1981).

20. M. Kurmoo and R.J.H. Clark, *Inorg. Chem.*, **24**, 4420 (1985).

21. R. Ikeda, T. Tamura and M. Yamashita, *Chem. Phys. Lett.*, **173**, 466 (1990).

22. E.J.W. Austin, P.J. Barrie and R.J.H. Clark, *Inorg. Chem.*, **31**, 4281 (1992).

23. E.J.W. Austin, P.J. Barrie and R.J.H. Clark, *Inorg. Chem.*, **34**, 3859 (1995).

Chapter 2

Spin Solitons in Halogen-Bridged 1-D Mixed Valence Complexes

2.1 Introduction

The halogen-bridged $-M^{2+}-X-M^{4+}-X-$ (M: Pt, Pd; X: Cl, Br, I) type mixed valence complexes have been studied as one-dimensional (1-D) electronic systems with Peierls distortion [1-31]. Characteristic properties of these complexes have been investigated by structural [2-15], optical [16-23] and magnetic resonance studies [24-31]. The presence of kink-type solitons reported in *trans*-polyacetylene has been theoretically predicted [32,33] in halogen-bridged complexes by noting alternating *d*-electron distribution made by the 1-D arrangement of M^{2+} and M^{4+} metal sites. It is expected that the neutral soliton is formed by inserting a paramagnetic M^{3+} site as $-X-M^{2+}-X-M^{4+}-X-M^{3+}-X-M^{2+}-X-M^{4+}-X-$. Magnetic resonance studies (NMR and ESR) have been reported on $[Pd(chxn)_2][PdBr_2(chxn)_2]Br_4$ (chxn: 1R,2R-cyclohexanediamine) [10,19,31] in order to reveal the dynamic behaviour of paramagnetic electron spins, and showed that electron spins rapidly diffuse along the chain just like in *trans*-polyacetylene explainable by the formation of neutral spin solitons [31].

In the present study, the temperature dependence of ESR spectra and the temperature and frequency dependences of ^1H NMR relaxation time T_1 were measured to investigate dynamic behaviour of paramagnetic sites formed in $[Pt(en)_2][PtBr_2(en)_2](ClO_4)_4$,

$[Pd(en)_2][PdBr_2(en)_2](ClO_4)_4$ and $[Pd(en)_2]$ $[PdCl_2(en)_2](ClO_4)_4$ (en: ethylenediamine).

The crystal structures in these three complexes were determined at room temperature by X-ray diffraction [6,7,9,11-13] as shown in Fig. 2-1. The chains are expected to be well isolated with each other because perchlorate ions located in the inter-chain form no marked hydrogen bond. At room temperature, the conformations of the two en chelate rings were shown to be λλ or δδ in $M(en)_2$ unit, and the chain structure which consists of $-M^{2+}-X-M^{4+}-X-$ can be expressed as the sequence ··· (λλ) (δδ) (λλ) (δδ) ···. In $[Pt(en)_2][PtBr_2(en)_2](ClO_4)_4$, it has been reported that the conformations of the en chelate rings are changed from λλ (δδ) to δλ (λδ) at a phase transition of 297.8 K from the high- to low-temperature phase [13].

In addition, to elucidate the existence of the solitons more in detail, the hetero-metal complexes $[Pd(en)_2][PtX_2(en)_2](ClO_4)_4$ (X: Cl, Br) which have non-degenerate electronic ground state is studied because the valence structure in the chain is expected to be $-Pd^{2+}-X-Pt^{4+}-X-$ [34-37] which can be shown from the energy level of 4*d* orbitals in Pd ions lower than that of 5*d* orbitals in Pt ions. From this non-degenerate structure, we can expect that the solitons become more difficult to be produced in this system. In this study, by comparing the ESR and NMR data performed in the hetero-metal complexes with data on the homo-metal complexes mentioned above, the stability conditions for soliton formation in the 1-D chain will be discussed.

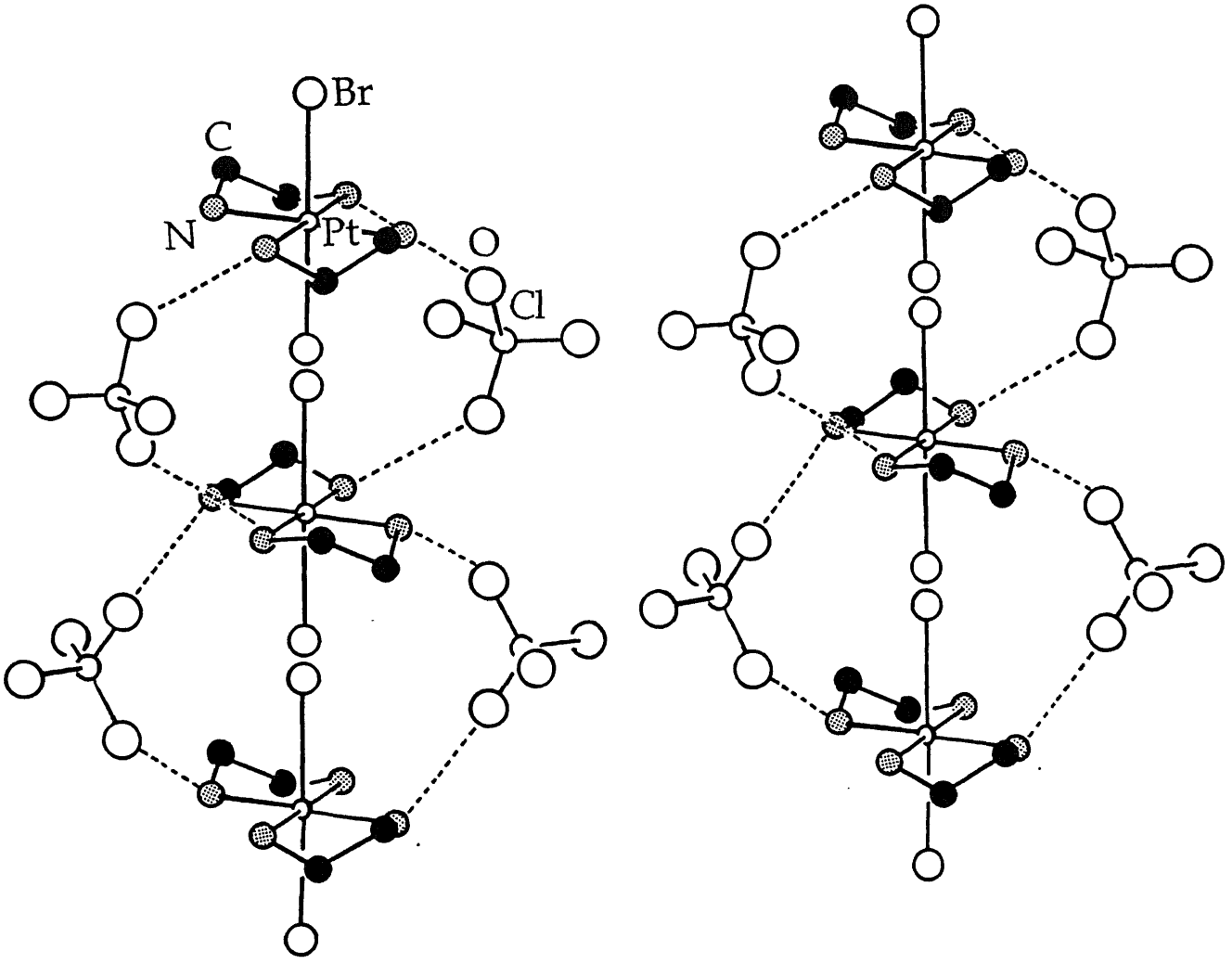

Fig. 2-1 The structure of a halogen-bridged one-dimensional complex, $[Pt(en)_2][PtBr_2(en)_2](ClO_4)_4$ determined by X-ray diffraction at 298 K [6,11-13]. The positions of the bridged bromine atoms are disordered over two sites in the chain.

2.2 Experimental

NMR, ESR and differential scanning calorimetry (DSC) measurements were performed on the crystals of $[Pt(en)_2][PtBr_2(en)_2](ClO_4)_4$, $[Pd(en)_2][PdX_2(en)_2](ClO_4)_4$ and $[Pd(en)_2][PtX_2(en)_2](ClO_4)_4$ (X: Cl, Br) prepared according to literature [1]. For the ^1H NMR measurement, the obtained crystals (*ca.* 1 g) was sealed in a glass ampoule under a dry nitrogen atmosphere. The ^1H spin-lattice relaxation time, T_1 in $[Pt(en)_2][PtBr_2(en)_2](ClO_4)_4$, $[Pd(en)_2][PdCl_2(en)_2](ClO_4)_4$ and $[Pd(en)_2][PtX_2(en)_2](ClO_4)_4$ were determined using the inversion and saturation recovery methods at Larmor frequencies 15- 60 MHz in a temperature range of 90- 330 K by a home-made pulsed spectrometer constructed with a Thamway A57-4702 wide-band power amplifier, Matec model 251 and 252 preamplifiers, an Aniritsu M40573 frequency synthesizer and JEOL JTR-310 or JES-CC2 electromagnets. The ^1H T_1 of $[Pd(en)_2][PdBr_2(en)_2](ClO_4)_4$ was measured using the inversion recovery method at 20- 300 MHz in 90- 300 K using the spectrometer mentioned above and a Bruker MSL-300 system. The sample temperature was controlled by the nitrogen gas flow system and determined by a chromel-constantan thermocouple within an accuracy of ± 1 K.

ESR spectra were obtained with an *X*-band JEOL JES-FE1XG spectrometer on powder samples under a modulation field of 10 G with the frequency of 100 kHz in a temperature range between 130 and 300 K. The variable-temperature measurement was made with a JEOL NM-PVT system. A sample was loaded into the

quartz ESR tube in dry nitrogen gas. The values of the spin concentration were determined by comparing the integrated intensity with that in DPPH (1,1-Diphenyl1-2-picrylhydrazyl) with a known concentration.

DSC was carried out using a Seiko instruments calorimeter (model DSC-120) in the temperature range between 170 and 350 K. The scanning rates were performed at 1- 3 K min^{-1}. Samples of 3- 10 mg sealed in aluminium vessels were used for the measurement.

2.3 Results and Discussion

2.3.1 $[Pt(en)_2][PtBr_2(en)_2](ClO_4)_4$

The ^1H NMR T_1 measurement carried out below the phase-transition temperature (T_{tr}= 297.8K [13]) showed a marked nonexponential behaviour of the ^1H magnetization recovery after a $\pi/2$ pulse in the whole Larmor frequency range investigated (15- 60 MHz). As an example, the recovery data observed at 90 K (42.79 MHz) is shown in Fig. 2-2. This curve can be roughly divided into two components exhibiting fast and slow relaxations. The temperature dependence of ^1H magnetization ratio of the fast to the slow component is shown in Fig. 2-3. Upon heating, the contribution from the fast component gradually decreased, and almost vanished in the neighbourhood of T_{tr} where only a single exponential recovery was obtained as shown in Fig. 2-4.

In the temperature range studied (90- 320 K), the magnetization from the slow component was always major and its recovery obtained by the inversion recovery method gave a single relaxation time T_1 as expressed as

$$M(\tau) = M_0[1 - 2\exp(-\frac{\tau}{T_1})], \qquad (2\text{-}1)$$

where M_0 and $M(\tau)$ are ^1H magnetizations after π- t -$\pi/2$ pulses observed in the limit of $t \rightarrow \infty$ and $t = \tau$, respectively. On the other hand, the fast or minor component showed

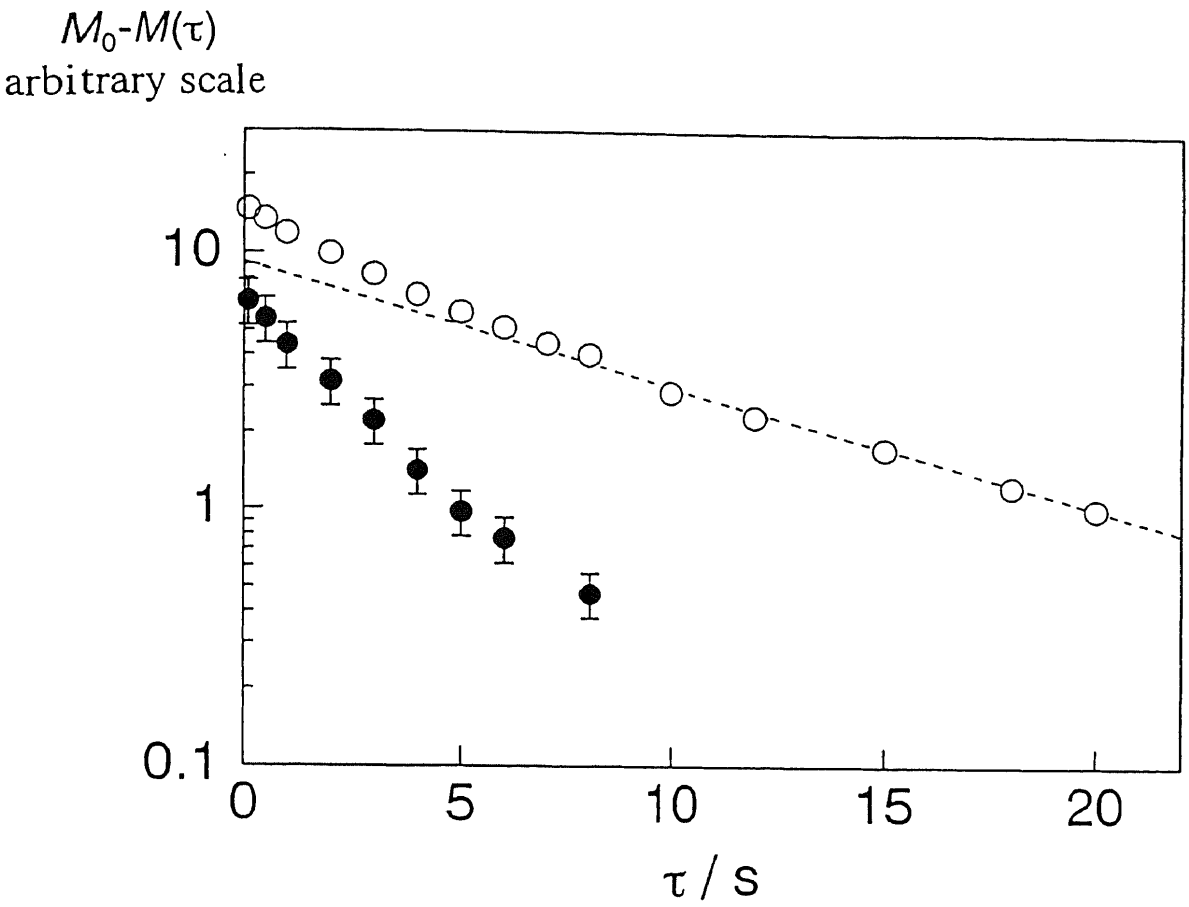

Fig. 2-2 The recovery of ^{1}H magnetization, [M_0-$M(\tau)$] (○) observed after a $\pi/2$ pulse at 90 K (42.79 MHz) in $[Pt(en)_2][PtBr_2(en)_2](ClO_4)_4$. The slope of the dotted line affords T_1 of 9.5 s for the slowly relaxing component. The fast magnetization component (●) is given by the difference between the observed magnetization and the dotted line.

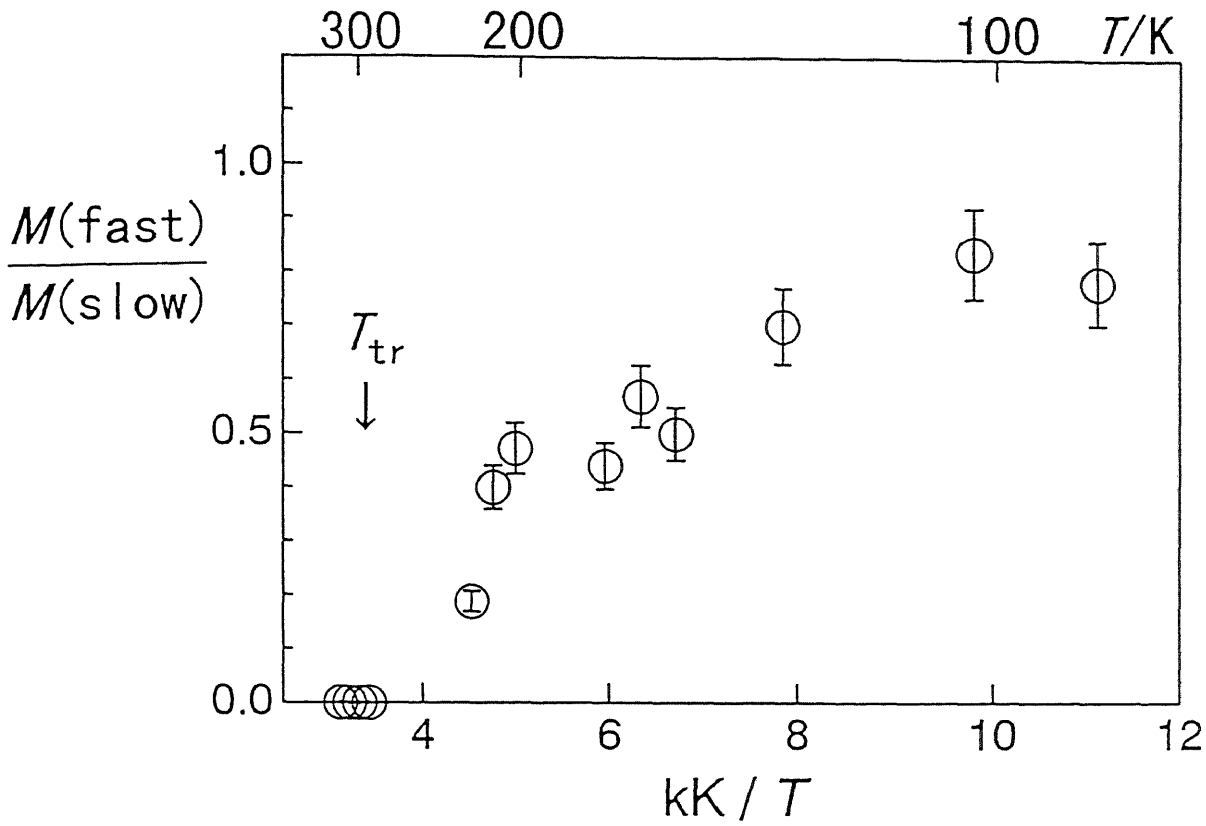

Fig. 2-3 A temperature dependence of the magnetization ratio, [M (fast) / M (slow)] of the fast to the slow recovering components observed at 40.14 MHz in $[Pt(en)_2][PtBr_2(en)_2](ClO_4)_4$. T_{tr} shows the phase transition temperature of 297.8 K [13].

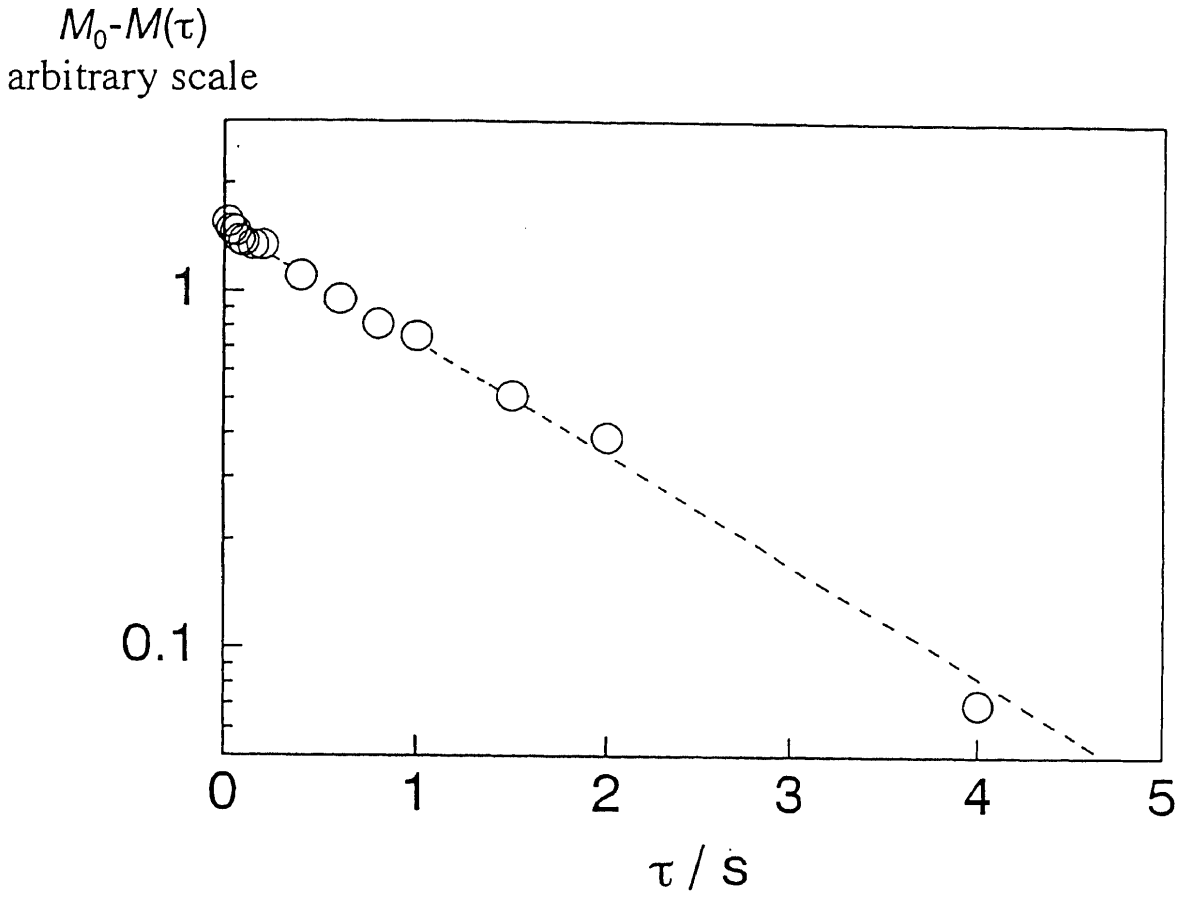

Fig. 2-4 The recovery of ^{1}H magnetization, [M_0-$M(\tau)$] observed at 321 K (40.14 MHz) in $[Pt(en)_2][PtBr_2(en)_2](ClO_4)_4$. The slope of the dotted line affords T_1= 1.35 s.

nonexponential recovery giving no single T_1.

The temperature dependence of T_1 of the slow component is shown in Fig. 2-5. Upon heating, T_1 decreased gradually up to *ca.* 250 K, then sharply to T_{tr}. After a sudden increase at T_{tr}, T_1 again showed a gradual decrease with further heating to 320 K.

The fast component can be assigned to the relaxation due to trapped or fixed paramagnetic Pt^{3+} sites on the chains and/or the chain ends in crystals. This is because proton spins located near such fixed Pt^{3+} sites feel a strong fluctuating of magnetic field made by the fixed electron spins, and since the magnitude of the fluctuation field depends upon the electron-proton distances distributed values of T_1 were obtained. In this case, the magnetization for the short duration time τ increases as the square root of τ when spin diffusion among protons is slow enough [38]. In fact, the fast component was roughly satisfied with this relationship supporting this interpretation of the paramagnetic relaxation mechanism as shown in Fig. 2-6.

For the protons far from the unpaired electrons, the paramagnetic field is so weakened that the spin-diffusion mechanism among the protons becomes the main process of the relaxation. Since the exponential T_1 behaviour is expected for these protons, the observed slow component is attributable to those protons remote from the paramagnetic electrons.

The decrease of the fast magnetization component observed with increasing temperature shown in Fig. 2-3 implies the decrease in the number of protons placed in

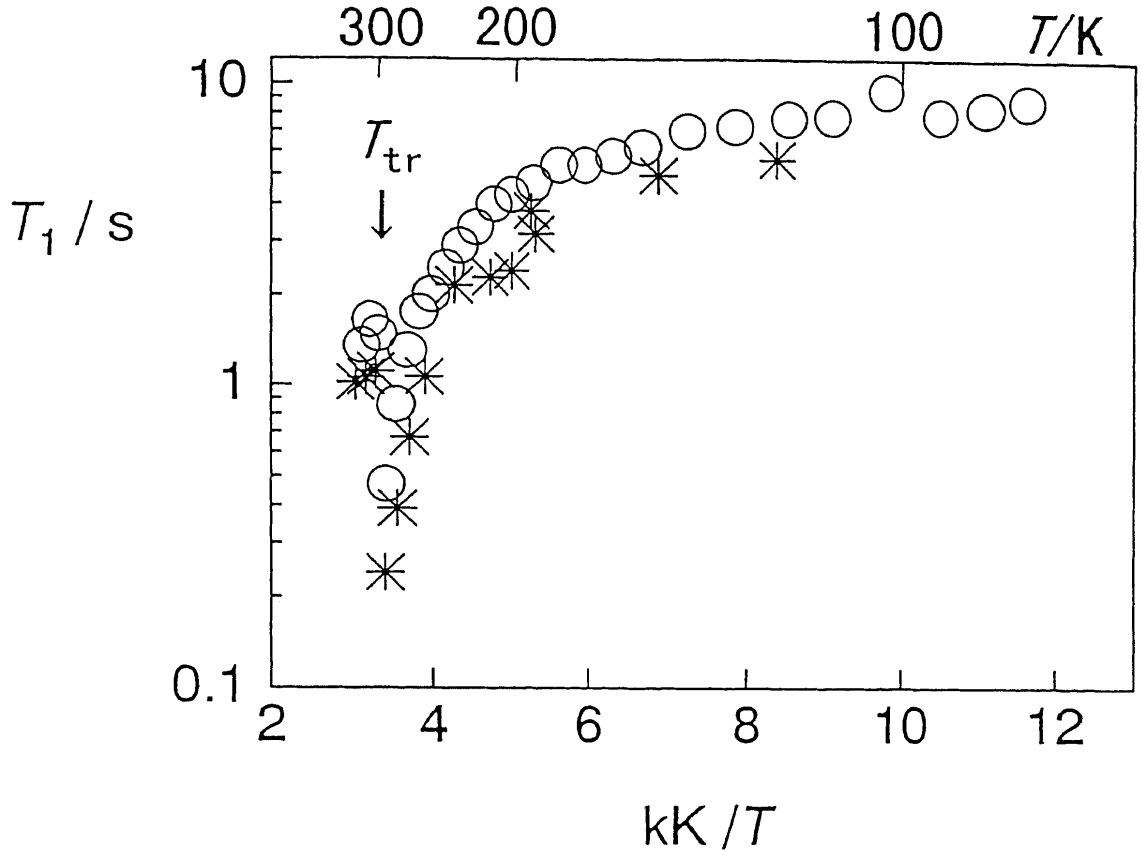

Fig. 2-5 Temperature dependences of ^1H T_1 observed at 20.96 (*) and 40.14 MHz (○) in $[Pt(en)_2][PtBr_2(en)_2](ClO_4)_4$. T_{tr} shows the phase transition temperature.

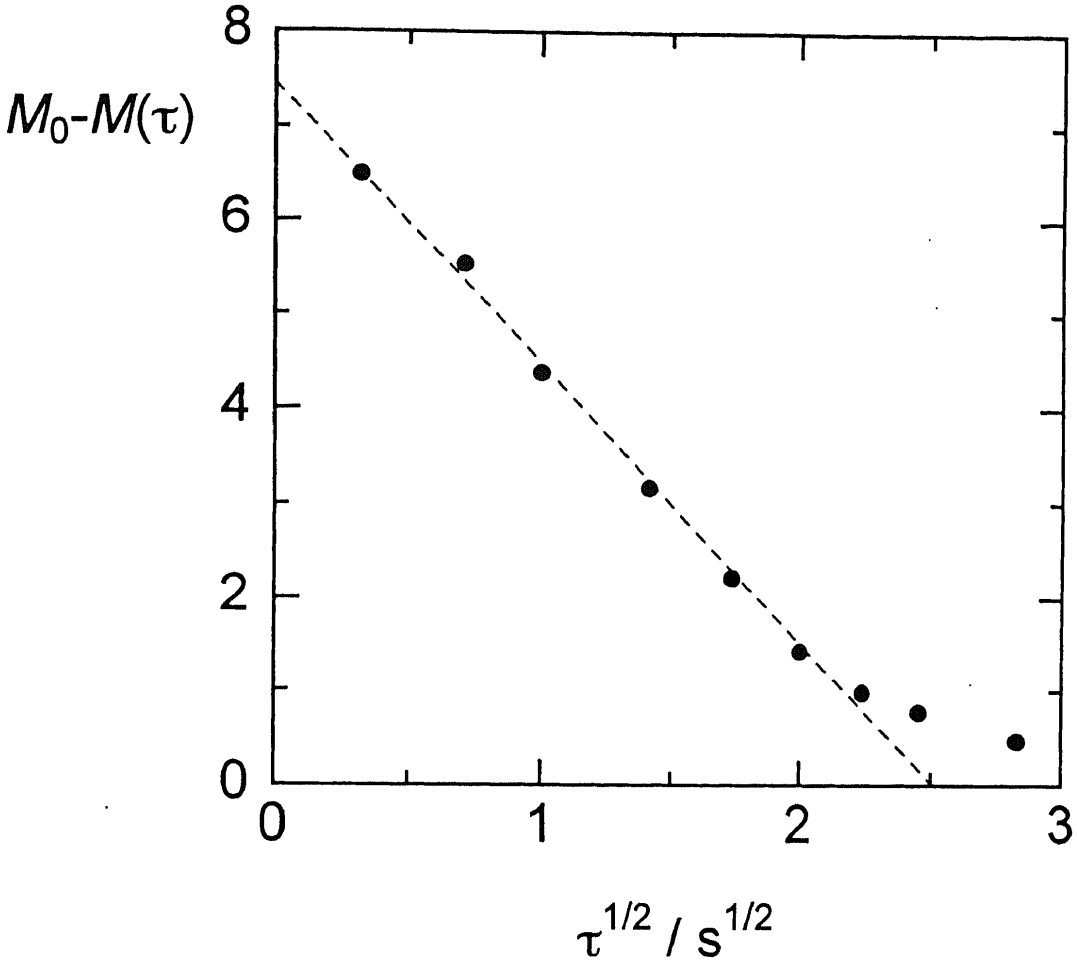

Fig. 2-6 The recovery of ^{1}H magnetization, [M_0-$M(\tau)$] of the fast relaxing component in $[Pt(en)_2][PtBr_2(en)_2](ClO_4)_4$ at 90 K (42.79 MHz) determined in Fig. 2-2. The broken line is fitted the magnetization proportional to the square root of the duration time τ.

the strong magnetic field made by the fixed paramagnetic spins. Since the paramagnetic Pt^{3+} density in crystals was reported to be temperature independent [25], this result suggests that, upon heating, the fixed paramagnetic sites decrease in number, that is, some of the fixed electron spins begin to move along the chain apart from the trapped sites by obtaining thermal excitation energies, and the number of moving electrons increases with temperature.

In case electron spins diffuse rapidly enough, the protons on the chain feel a averaged magnetic field made by the electrons. This reduces T_1 of the protons which are located far from electrons and their relaxation is controlled by the spin diffusion at low temperatures. In fact, the temperature dependence of T_1 in the slow component given in Fig. 2-5 shows a gradual shortening of T_1 upon heating implying that the contribution from the diffusing electron-spin to ^1H relaxation (slow component) increases with temperature. At the same time, the decrease of trapped electrons with increasing temperature reduces the fast magnetization component in conformity with the data shown in Fig. 2-3. The present model of the electron-spin migration can be supported by the temperature dependence study [25] of the ESR linewidth which showed a gradual narrowing upon heating attributable to the motional effect.

The dimensionality of the electron-spin motion was investigated by measuring the Larmor-frequency dependence of ^1H T_1. Devreux *et al.* have reported [39-41] that the nuclear relaxation due to the fluctuation of the magnetic field made by

the randomly jumping electron spins under the condition that the diffusion rate fulfills D^* » ω_e, ω_N where ω_e and ω_N are electron and nuclear Larmor frequencies, respectively, can be given by

$$T_1^{-1} = kT\chi_s[\frac{3}{5}d^2 f(\omega_N) + (a^2 + \frac{7}{5}d^2) f(\omega_e)], \tag{2-2}$$

where $f(\omega)$ denotes the spectrum density, and in case of 1-D, 2-D and 3-D systems with three different diffusion rates of D_1^*, D_2^* and D_3^* in the same order where $D_1^* \geqq D_2^* \geqq D_3^*$ are, respectively, expressed as

$$f(\omega)_{1\text{-D}} = \frac{1}{\sqrt{2D_1^* \omega}} \qquad (D_1^* > \omega > D_2^*, D_3^*), \tag{2-3}$$

$$f(\omega)_{2\text{-D}} = \frac{1}{2\pi\sqrt{D_1^* D_2^*}} \ln\frac{4\pi^2 D_2^*}{\omega} \qquad (D_1^*, D_2^* > \omega > D_3^*) \tag{2-4}$$

and

$$f(\omega)_{3\text{-D}} = \frac{1}{2\pi\sqrt{D_1^* D_2^*}} \ln\frac{4e^2 D_2^*}{D_3^*} \qquad (D_1^*, D_2^*, D_3^* > \omega). \tag{2-5}$$

Here, d and a are anisotropic (dipolar) and isotropic (scalar) parts of the hyperfine

coupling between protons and electrons, respectively. χ_s denotes the normalized electron susceptibility per Pt site given by [40]

$$\chi_s = \frac{\chi_m^s}{N_A g^2 \mu_B{}^2}, \tag{2-6}$$

where $\chi^s{}_m$ and g are the molar susceptibility and the powder average ($g = (2g_\perp + g_{//}) / 3$) of the g-factors $g_\perp$ and $g_{//}$, respectively. In case the electron spin are not localized but distributed along the chain, the function of spectrum density $f(\omega)_{1\text{-D}}$ in the 1-D model is expressed as [41]

$$f(\omega)_{1\text{-D}} = \frac{1}{\sqrt{2D_1^* \omega}} - \frac{C}{2D_1^*}, \tag{2-7}$$

where C represents a constant depending upon the delocalization length of the electron spin diffusing and is written by

$$C = 2\gamma\lambda, \tag{2-8}$$

where γ is given by 0.33 when $\lambda > 5$, and λ is called the delocalization length. D_1^* is

defined using the 1-D diffusion constant D_1 and the inter-site distance b in the chain as

$$D_1^* = \frac{D_1}{b^2}, \tag{2-9}$$

where D_1^* and D_1 will be termed as D^* and D henceforth.

Here, it is assumed that the coupling is approximately dipolar because no hydrogen is directly bound to paramagnetic Pt^{3+} atoms, then Eq. (2-2) is rewritten as

$$T_1^{-1} \cong kT\chi_s[\frac{3}{5}d^2 f(\omega_N) + \frac{7}{5}d^2 f(\omega_e)]. \tag{2-10}$$

Using the data on the crystal structure, the dipolar coupling constant d can be calculated by use of the equation:

$$d^2 = \frac{1}{N_H} h^2 \gamma_e^2 \gamma_H^2 \sum_i^{N_H} \sum_j r_{ij}^{-6}, \tag{2-11}$$

where N_H is the number of crystallographically nonequivalent protons, r_{ij}, the distance between the j-th protons and the i-th mixed-valence Pt^{2+} or Pt^{4+} site, and γ_e and γ_H, electronic and protonic magnetogyric ratios. Putting Eq. (2-7) into Eq. (2-10), the proton T_1 contributed from the 1-D diffusion of electron spins can be finally written as

$$T_1^{-1} = kT\chi_s \frac{d^2}{5}[(3+7\sqrt{\frac{\gamma_H}{\gamma_e}})(2D^*\omega_H)^{-\frac{1}{2}} - \frac{5C}{D^*}] \ . \qquad (2\text{-}12)$$

The Larmor frequency dependences of T_1 observed at 125 and 303 K are shown in Fig. 2-7. The observed T_1^{-1} versus $\omega_H^{-1/2}$ plots can be well interpreted by Eq. (2-12), by supporting the 1-D diffusion of electron spins. From the slope of the plots, the diffusion rate D^* can be estimated in the whole temperature range studied. In this caluculation, d^2 was evaluated as 4.5×10^{14} rad^4 s^{-2} by substituting the data of crystal structure [13] into Eq. (2-11). The values of χ_s at various temperatures were estimated by assuming that the concentration of the diffusing electron-spins is proportional to the magnetization of the slow component given in Fig. 2-3. Calculating χ_s using this assumption, the temperature dependence of D^* was obtained as shown in Fig. 2-8. D^* values increased gradually from 4 to 10×10^{12} rad s^{-1} upon heating from 90 to 180 K, then decreased on heating to T_{tr}. Since the linear temperature dependence observed below *ca.* 180 K can be expressed using an Arrhenius equation as

$$D^* = D_0^* \exp(\frac{-E_a}{kT}), \qquad (2\text{-}13)$$

where D_0^* and E_a denote the diffusion rate at the limit of infinite temperature and the activation energy for electron-spin migration along the chain, respectively, E_a was

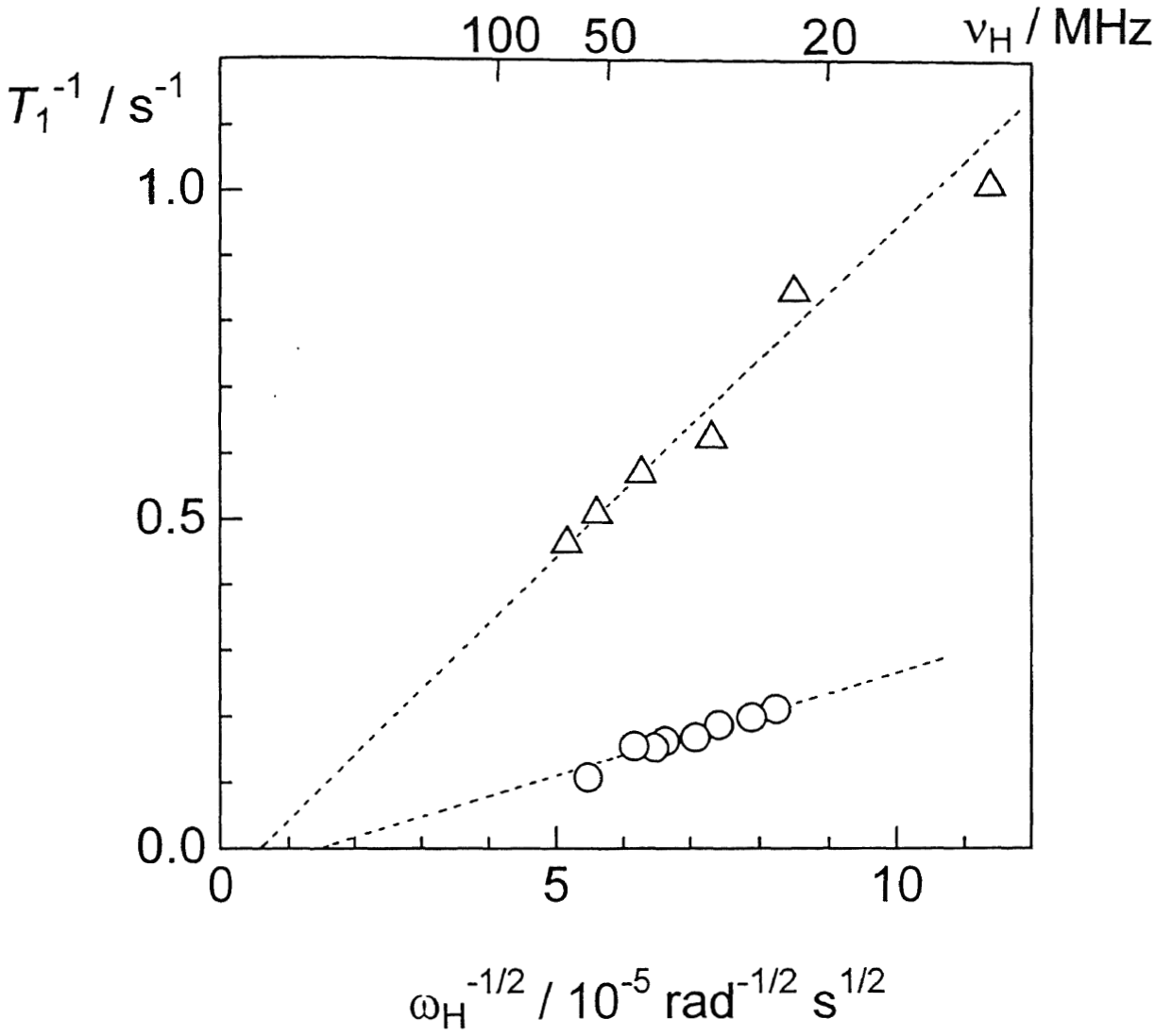

Fig. 2-7 Larmor frequency dependences of T_1 of the slowly relaxing components observed at 125 (○) and 303 K (△) in $[Pt(en)_2][PtBr_2(en)_2](ClO_4)_4$. Dotted lines are fitted theoretical T_1 proportional to the square root of the Larmor frequency ν_H (angular frequency ω_H) (see text).

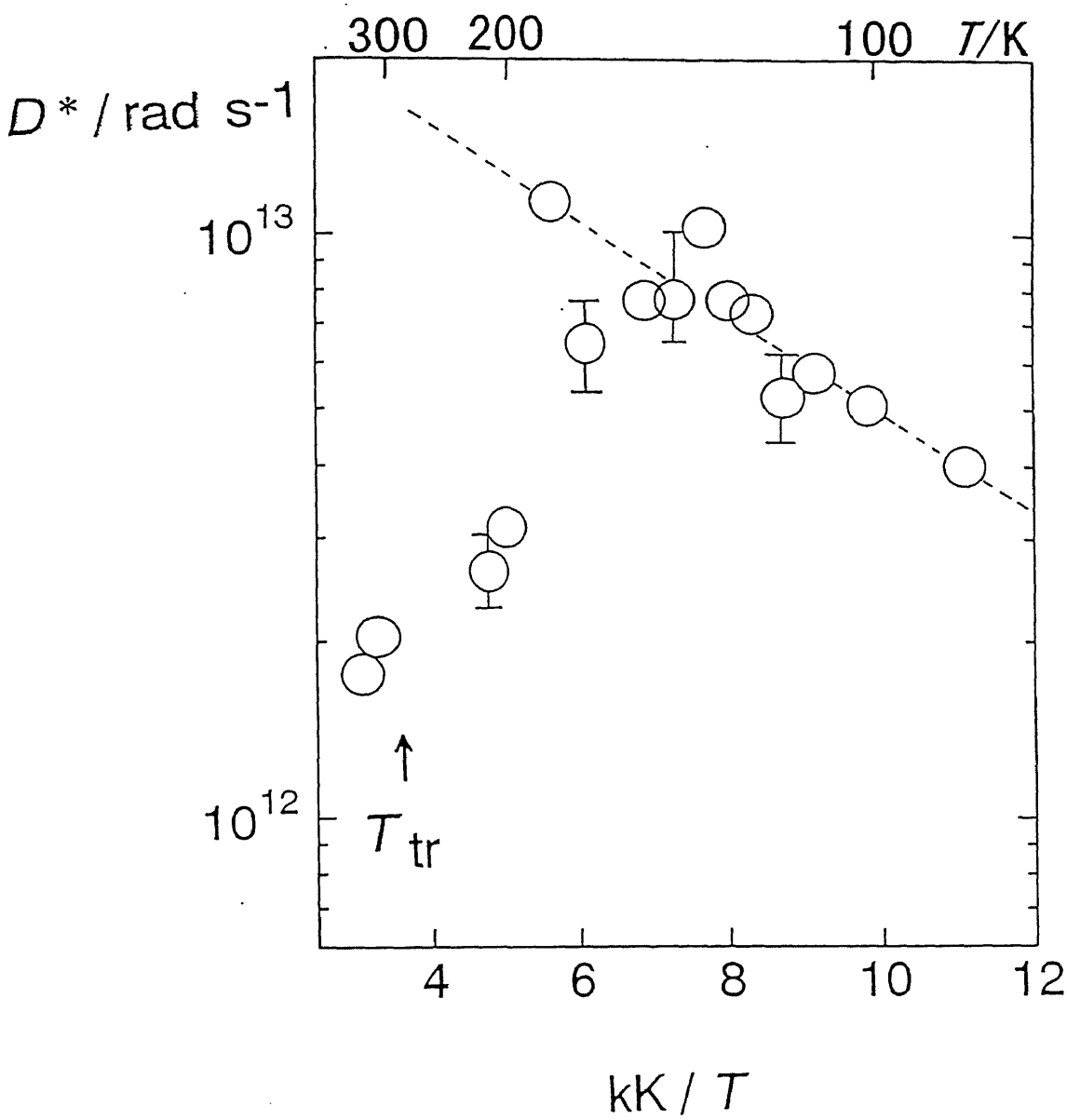

Fig. 2-8 The temperature dependence of 1-D spin diffusion rate D^* of electron spins observed in $[Pt(en)_2][PtBr_2(en)_2](ClO_4)_4$. The slope of the dotted line which indicates the best-fit theoretical values gives an activation energy of 17±2 meV. T_{tr} shows the phase transition temperature.

estimated to be 17±2 meV (1.6±0.2 kJ mol^{-1}) in this temperature range.

It is noted that this E_a value is quite small compared with E_a= 840 meV derived from the electrical conductivity measurement [42]. This difference can be explained as follows: Assuming that the unpaired spin and the charge-carrier have the same diffusion rate, the conductivity σ_{NMR} along the chain is expressed as the Nernst-Einstein relation [43-45] given by

$$\sigma_{NMR} = \frac{ne^2b^2D^*}{kT}. \qquad (2\text{-}14)$$

Here, n and e are the charge carrier concentration and the electronic charge, respectively. Substituting n= 10^{-4} per Pt site derived from the ESR data [25] and b= 5.5 Å [13] into Eq.(2-14), σ_{NMR}= 10^{-3} S cm^{-1} was evaluated at 303 K. This value is seven orders of magnitude larger than the measured value of 10^{-10} S cm^{-1} [42]. This comparison between the NMR and electrical conductivity results implies that the carriers of spin and charge should be different in the present system. The diffusing spin carriers detected from ^1H T_1 are, accordingly, mostly explained by the model of neutral solitons as shown in Fig. 2-9, where the unpaired electron spin on Pt^{3+} site migrates from right to left, whereas the electrons alternately migrate left and right, respectively from Pt^{3+} to Pt^{4+} and from Pt^{2+} to Pt^{3+}, as shown by the double line arrows. Since this motion contributes no bulk electric current, we can say that the soliton diffusion is accompanied no electron conductivity.

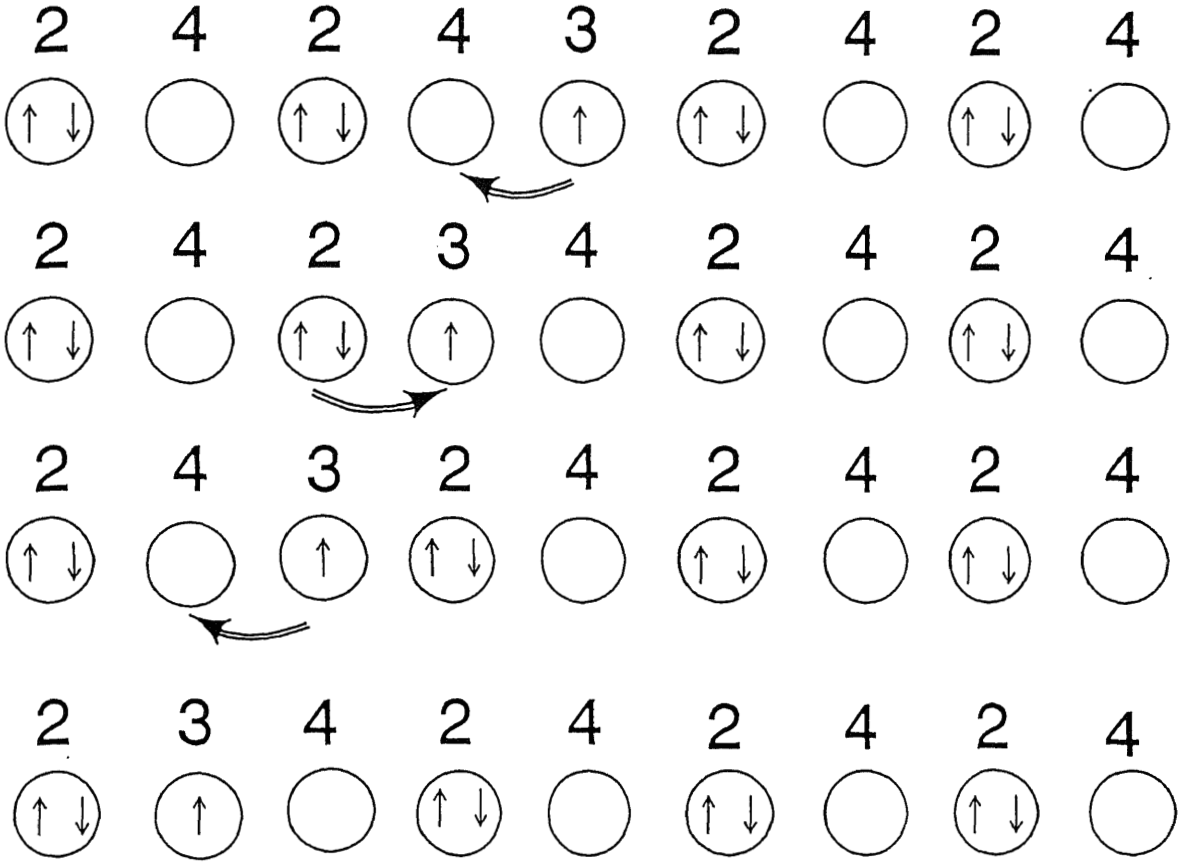

Fig. 2-9 An acceptable neutral soliton model of spin migration along 1-D chain. The numbers 2, 3 and 4 represent Pt^{2+}, Pt^{3+} and Pt^{4+} sites, respectively. Arrows in the circles are spins in the d_z^2 orbital. The double arrows represent the migration of electrons in the chain.

2.3.2 $[Pd(en)_2][PdBr_2(en)_2](ClO_4)_4$

The ESR signals observed in powder samples at three typical temperatures studied (133, 213 and 293 K) are shown in Fig. 2-10. These signals with anisotropy are ascribed to the paramagnetic Pd^{3+} sites on the chain. The peak to peak linewidth ΔH_{pp} obtained from in the derivative curve was gradually reduced with increasing temperature. The ΔH_{pp} in powder spectra originates mostly from the anisotropy of g-factors convoluted with the linewidth of each fine crystal. Assuming that the anisotropy of g-factors is independent of temperature, ΔH_{pp} with the narrowing effect could be roughly expressed as Arrhenius-type relationship given by

$$\Delta H_{pp} \cong \Delta H_0 + \Delta H_0' \exp(\frac{\Delta \varepsilon}{kT}), \tag{2-15}$$

where ΔH_0, ΔH_0' and $\Delta \varepsilon$ denote the anisotropy linewidth, the single crystal linewidth at the limit of infinite temperature and the activation energy, respectively. In the temperature range investigated, $\Delta \varepsilon$ is estimated to be *ca.* 14 meV. This behaviour can be explained by the motional narrowing effect of the thermally excited electron spins in the crystal. The temperature dependence of the molar spin susceptibility χ'_m obtained from the ESR signals is presented in Fig. 2-11. In the whole temperature range, χ'_m almost follows the Curie law given by

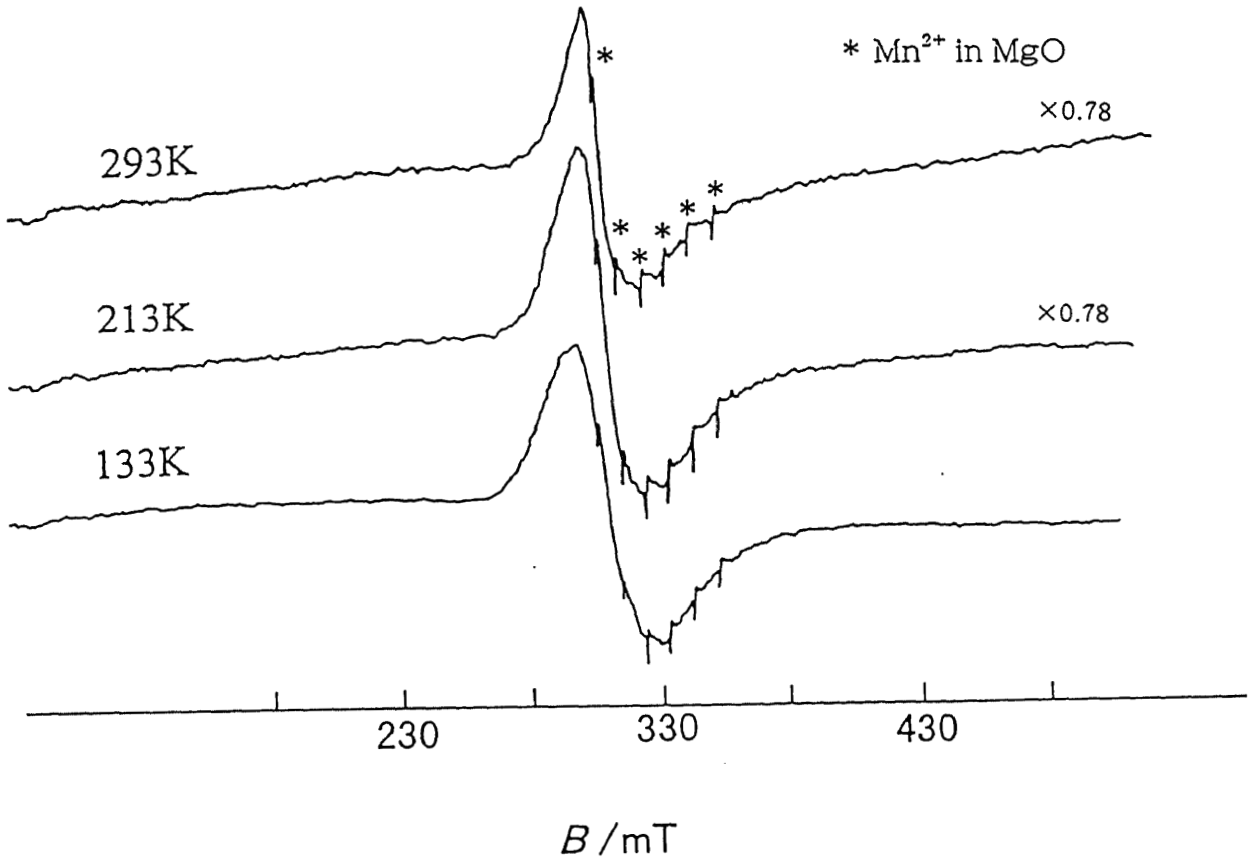

Fig. 2-10 The temperature dependence of derivative curves of ESR spectra for a powder sample of $[Pd(en)_2][PdBr_2(en)_2](ClO_4)_4$. The lines with asterisks are the marker signals from doped Mn^{2+} in MgO.

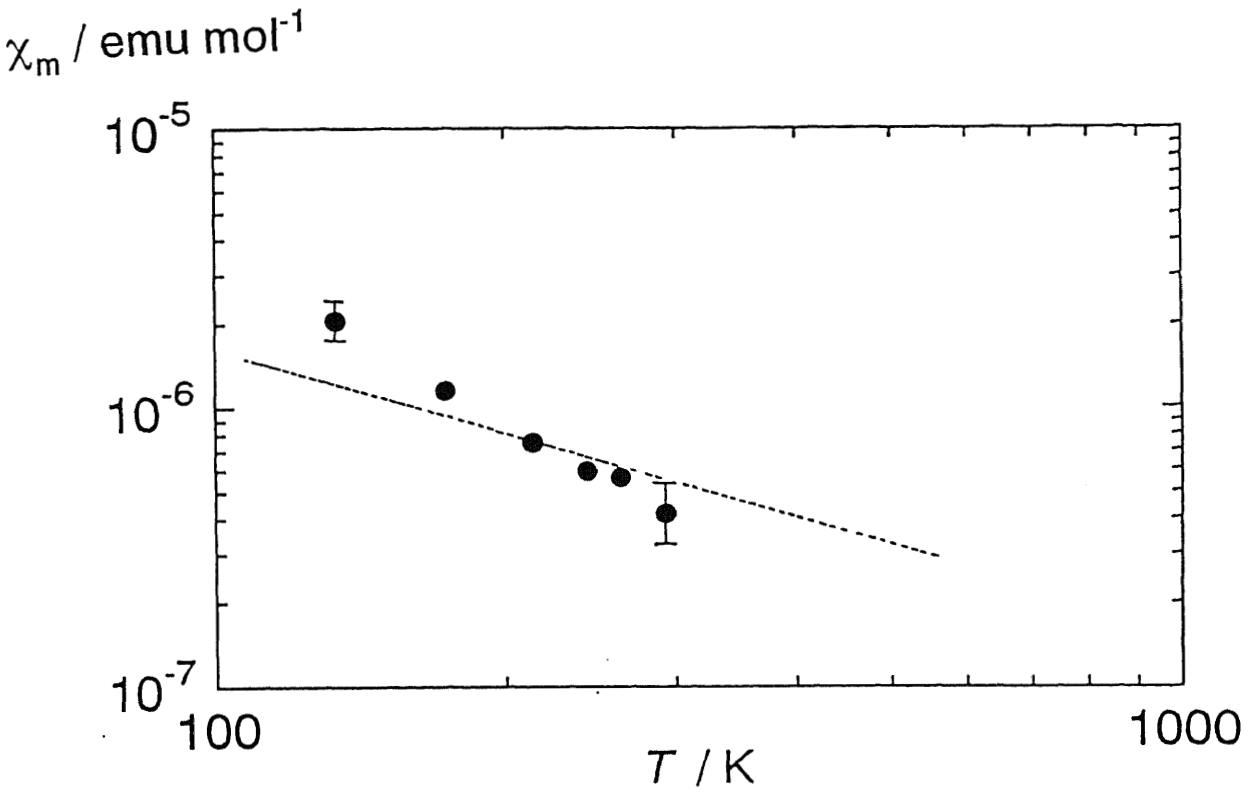

Fig. 2-11 The temperature dependence of the molar spin susceptibility χ'_m derived from ESR intensities in $[Pd(en)_2][PdBr_2(en)_2](ClO_4)_4$. The dotted line represents the component following the Curie law.

$$\chi^{s}_{m} = \frac{C_C}{T}, \tag{2-16}$$

where C_C has been known as the Curie constant and expressed as

$$C_C = \frac{Ng^2\mu_B{}^2 S(S+1)}{3k}. \tag{2-17}$$

The present result indicates that a constant number of noninteracting Pd^{3+} spins exists in the chain. This concentration of Pd^{3+} spins is estimated to be *ca.* 10^{-4} per Pd site, and is close the reported value of 2.8×10^{-4} [25] in $[Pt(en)_2][PtBr_2(en)_2](ClO_4)_4$.

In the ^1H NMR T_1 measurement, the magnetization after a π- τ -$\pi/2$ pulse sequence afforded a marked nonexponential recovery in whole frequency range studied. This recovery was more serious at low temperatures. Three examples for the observed data are shown in Fig. 2-12. The observed recovery curve was roughly divided into two components showing fast and slow relaxations in the low-temperature range. The contribution from the fast component decreases upon heating, and almost vanished above the phase-transition temperature T_{tr} of 279 K determined by the DSC measurement reported in literature [13], and only a single exponential recovery was observed as shown at 291 K in Fig. 2-12.

In the whole temperature range studied, the slow magnetization component

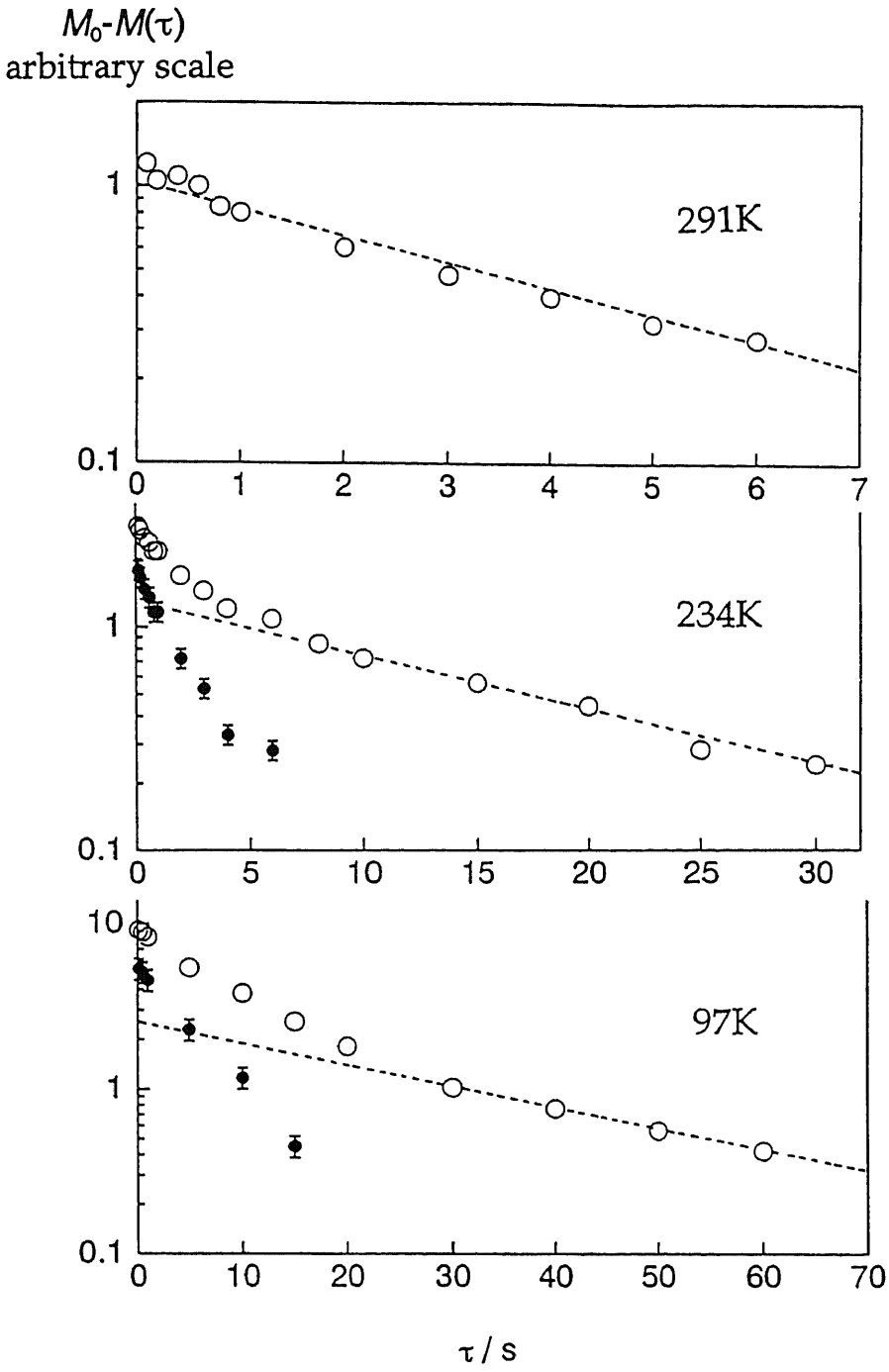

Fig. 2-12 Recoveries of ^{1}H magnetization, [M_0-$M(\tau)$] (○) observed at a Larmor frequency of 40.4 MHz in $[Pd(en)_2][PdBr_2(en)_2](ClO_4)_4$. The slope of dotted lines affords the T_1 of the slow-relaxing component. The fast magnetization components (●) are given by the difference between the observed magnetization and the dotted line.

showed almost a single exponential recovery providing a unique T_1, while the fast component always showed multi- exponential recovery giving no definite T_1 values. The temperature dependence of the long T_1 obtained from Eq. (2-1) is shown in Fig. 2-13. Upon heating, T_1 decreased gradually up to *ca.* 200 K, then sharply to T_{tr}. After a drastic jump at T_{tr}, T_1 again showed a slow decrease with a further heating to 300 K.

These relaxation data can be explained as follows: The temperature-independent Pd^{3+} sites with a concentration of *ca.* 10^{-4} revealed by the ESR measurement give the fluctuation of magnetic field strong enough to contribute to the ^1H relaxation. At a sufficient low temperature, it is expected that the Pd^{3+} sites are trapped at defect sites formed along the chains and/or at the chain ends in crystals. In this state, protons located near a Pd^{3+} site feel the fluctuation of strong magnetic field made by the electron magnetic moment where its magnitude depends upon the proton- electron distance (R). If the magnetic dipolar interaction is considered, ^1H T_1 is proportional to R^6 in the neighbourhood of the electron where the spin-diffusion among protons is ignorable [38]. For these protons, there should be a distribution of T_1 which agrees well with the nonexponential behaviour observed for the fast component. The decrease of the fast-relaxation magnetization observed with increasing temperature is attributed to the decrease in the number of protons placed in the strong fluctuation of magnetic field around the fixed paramagnetic spins.

On the other hand, the slow component with a definite T_1 value is

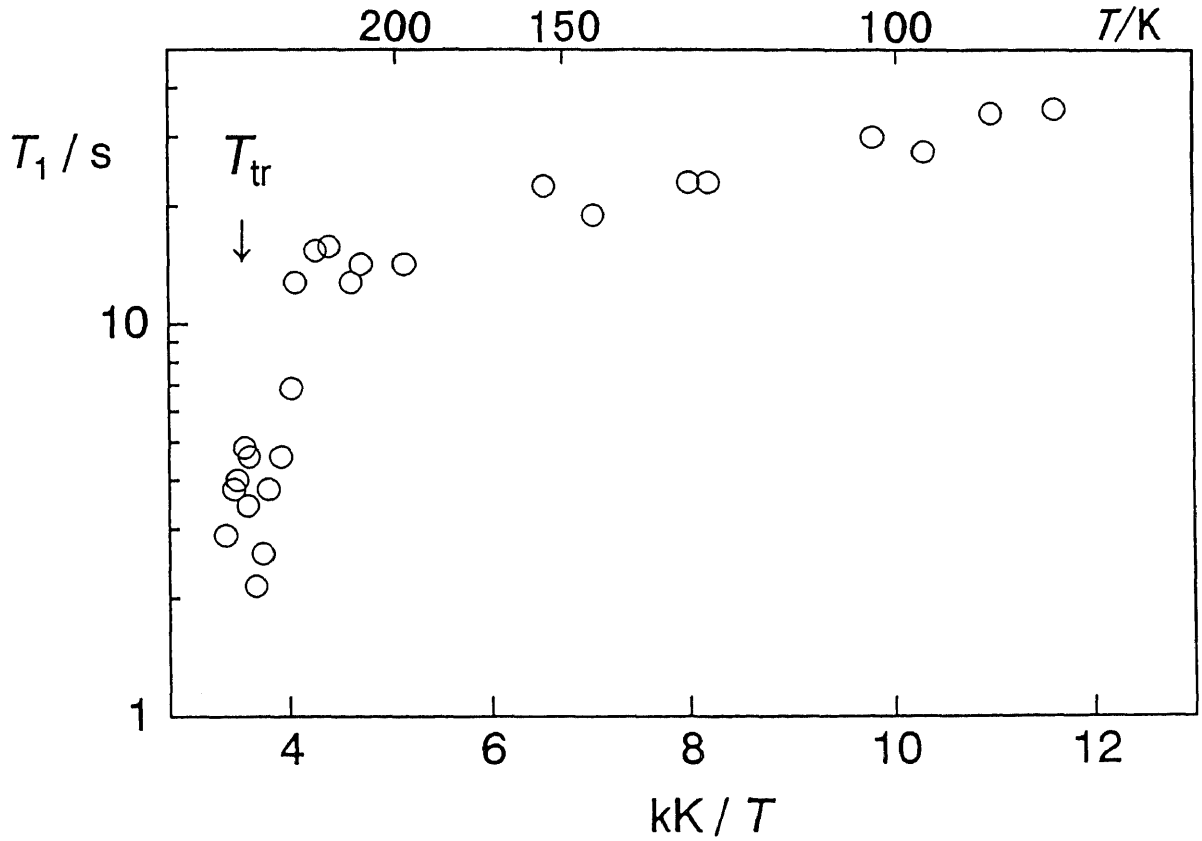

Fig. 2-13 A temperature dependence of ^1H T_1 observed at 40.4 MHz in $[Pd(en)_2][PdBr_2(en)_2](ClO_4)_4$. T_{tr} is the phase-transition temperature of 279 K by DSC measurement reported in the literature [13].

attributable to rapidly diffusing electron spins, which gives an averaged magnetic field fluctuation at the position of protons located over a wide range along the chains. In fact, the temperature dependent T_1 given in Fig. 2-13 showed a gradual shortening upon heating, and this result implies that the contribution from the diffusing spins to slow relaxation component increases with temperature.

The dimensionality of the electron-spin motion can be investigated by measuring the Larmor-frequency dependence of ^{1}H T_1. As discussed in Section 2.3.1, provided the electron spins rapidly diffuse along the chain, the proton T_1 due to magnetic field fluctuation made by the randomly hopping electron spins along the 1-D lattice is proportional to the square root of the Larmor frequency as given by Eq. (2-12). The frequency dependence of T_1^{-1} observed at 91, 200 and 287 K are shown in Fig. 2-14. It is noted that the observed T_1^{-1} versus $\omega_H^{-1/2}$ plots are well expressed by Eq. (2-12), supporting the present interpretation of T_1. The diffusion rate D^* and the delocalization parameter C can be estimated from the slope of plots and the intercept on the $\omega_H^{-1/2}$ axis, respectively. In Eq. (2-12), χ_s is roughly evaluated from Eqs. (2-6), (2-16) and (2-17), by assuming that the temperature dependence of the concentration N_D of diffusing spins can be expressed as

$$N_D = N_0 \exp(\frac{-\Delta\varepsilon}{kT}), \tag{2-18}$$

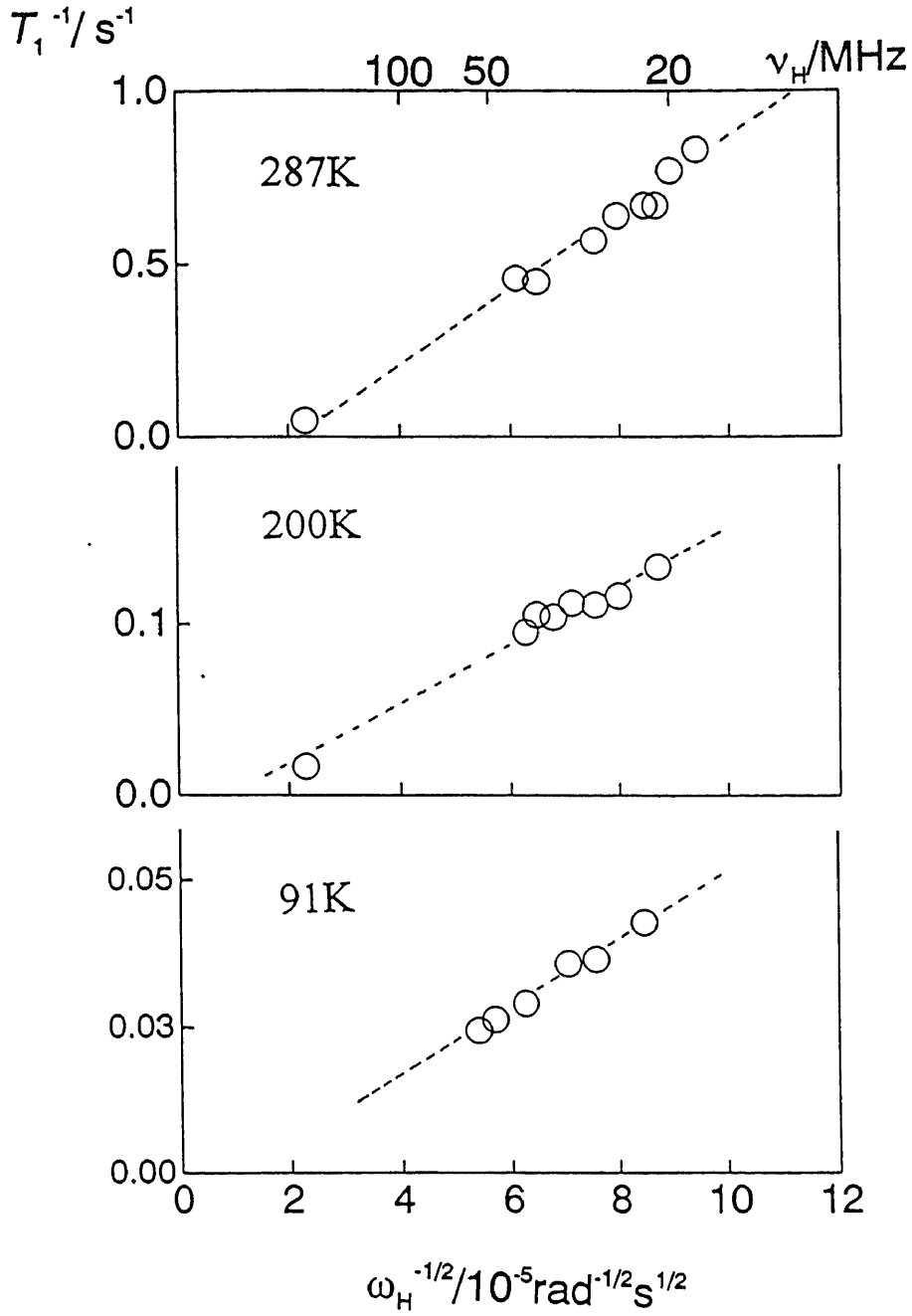

Fig. 2-14 Larmor frequency(ω_H) dependences of ^{1}H T_1 of the slow components observed in $[Pd(en)_2][PdBr_2(en)_2](ClO_4)_4$. Dotted lines have a linear relations with the square root of the Larmor frequency ν_H (angular frequency ω_H).

where N_0 and $\Delta\varepsilon$ are the total (fixed and diffusing) spin concentration given by *ca.* 10^{-4} and the activation energy for the spin motion of *ca.*14 meV (= 1.4 kJ mol^{-1}) given in Eq. (2-15), respectively, both are derived from the foregoing ESR result. Calculating χ_s using this assumption, and the d value of 4.5×10^{14} rad^4 s^{-2} which was evaluated by substituting the reported crystal data [13] into Eq. (2-11), the temperature dependence of D^* was evaluated and is shown in Fig. 2-15. Below *ca.* 200 K, D^* can be expressed as Eq. (2-13) with $D_0^*= 4.5\times10^{13}$ rad s^{-1} and $E_a= 7.5\pm4$ meV (= 0.72 ± 0.4 kJ mol^{-1}).

Using Eq.(2-8), the spin-delocalization lengths λ were calculated to be 20 at 91 K, 12 at 122 K, 26 at 142 K, 6 at 200 K and 8 Pd sites at 287 K, respectively. Since λ is considered to be temperature independent, its value was roughly evaluated to be 15 ± 10 Pd sites on the average. This value can be compared with the reported values (λ= *ca.* 17) for undoped *trans*-polyacetylene [46] and (λ= *ca.* 20) for $[Pd(chxn)_2][PdBr_2(chxn)_2]Br_4$ (chxn:1R,2R-cyclohexanediamine) [31] and the theoretically derived values of λ= *ca.* 12 for halogen-bridged mixed-valence complexes [47-49]. Assuming that the unpaired spin and the charge-carrier have the same diffusion rate, the conductivity along the chain is estimated to be *ca.* 10^{-2} S cm^{-1} at 287 K using the Nernst-Einstein relation given by Eq. (2-14). This value is six orders of magnitude larger than the measured value of 10^{-8} S cm^{-1} [42]. The carriers of spin and charge are, accordingly, different in the present system suggesting that the spins form neutral solitons in conformity with the model illustrated in Fig. 2-9.

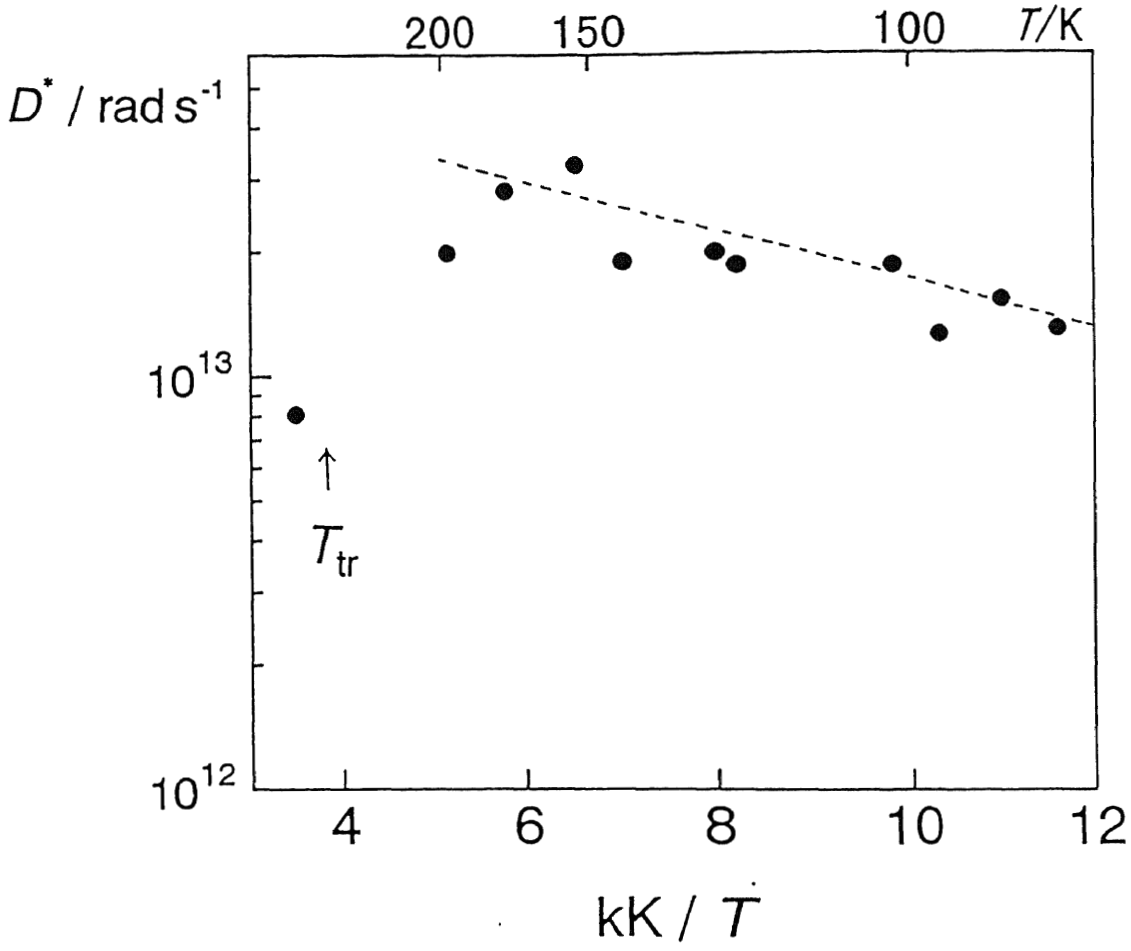

Fig. 2-15 The temperature dependence of 1-D diffusion rate D^* of electron spins determined in $[Pd(en)_2][PdBr_2(en)_2](ClO_4)_4$. The slope of the fitted dotted line gives an activation energy of 7.5±4 meV. T_{tr} is the phase-transition temperature of 279 K [13].

2.3.3 $[Pd(en)_2][PdCl_2(en)_2](ClO_4)_4$

The DSC measurement revealed a phase transition at 263 ± 1 K with a transition enthalpy of *ca.* 11 kJ mol^{-1}. This transition temperature is in good agreement with that determined by the measurement of temperature dependence of X-ray lattice parameters [13].

In the whole temperature range studied, the ESR spectra measurement revealed the presence of paramagnetic Pd^{3+} sites whose concentration showed an almost temperature independent value of 10^{-4}- 10^{-5} in molar ratio to that of the normal Pd^{2+} and Pd^{4+} sites.

^1H magnetization after a $\pi/2$ pulse afforded a marked nonexponential recovery over the whole frequency range (20- 55 MHz) studied as shown Fig. 2-16. This recovery was more serious at low-temperatures. The observed recovery curve was roughly divided into two components with fast or minor and slow or major relaxations. The temperature dependence of magnetization ratio of the fast to slow component is shown in Fig. 2-17. The contribution from the short component decreases upon heating, and vanished above the phase-transition temperature (T_{tr}) and only a single exponential recovery was obtained.

In the whole temperature range, the slow component showed almost exponential recovery, which can provide definite T_1 values, whereas the fast component always showed nonexponential recovery and could give no accurate T_1 values. This

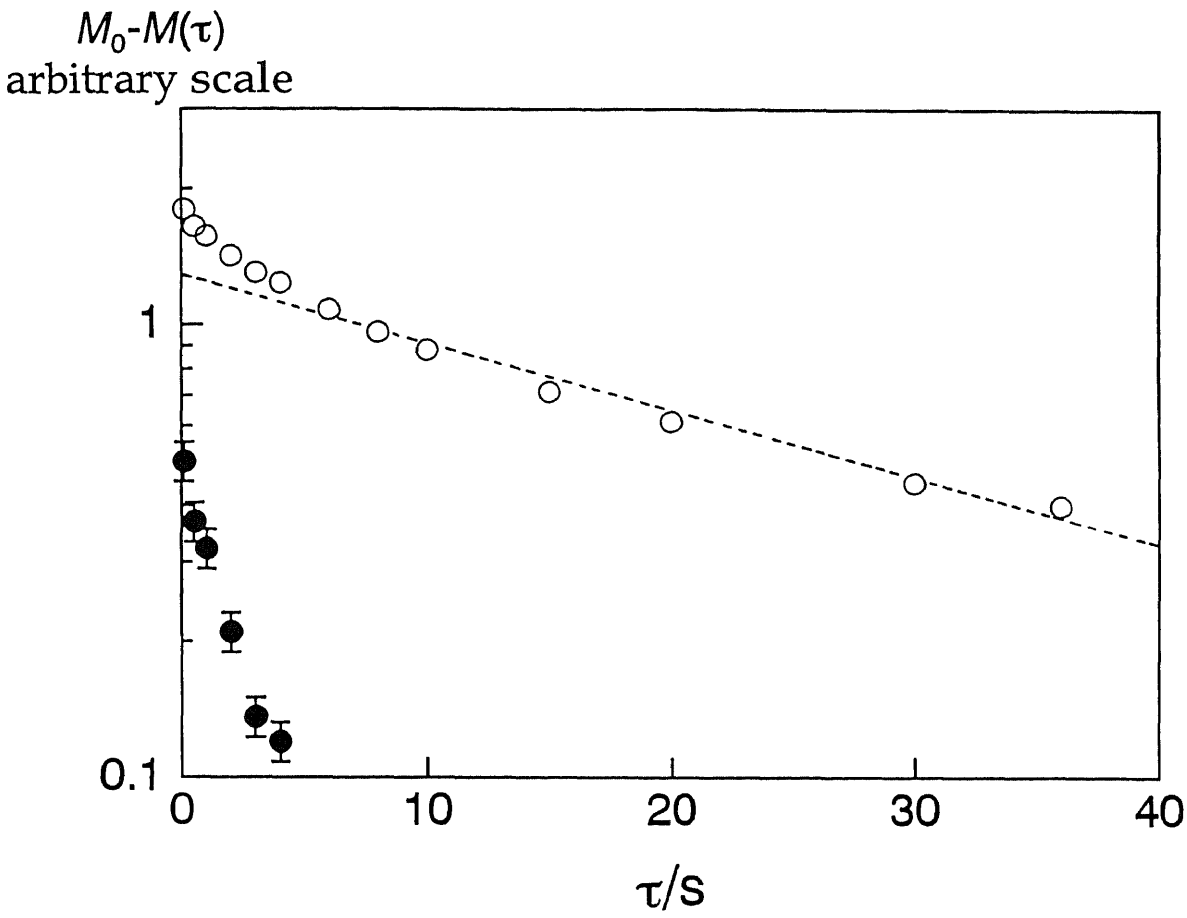

Fig. 2-16 The recovery of ^{1}H magnetization, [M_0-M (τ)] (○) observed at 83 K (54.27 MHz) in $[Pd(en)_2][PdCl_2(en)_2](ClO_4)_4$. The slope of dotted line affords T_1 of 27 s of the slow relaxing component. The fast magnetization component (●) is given by the difference between the observed magnetization and the dotted line.

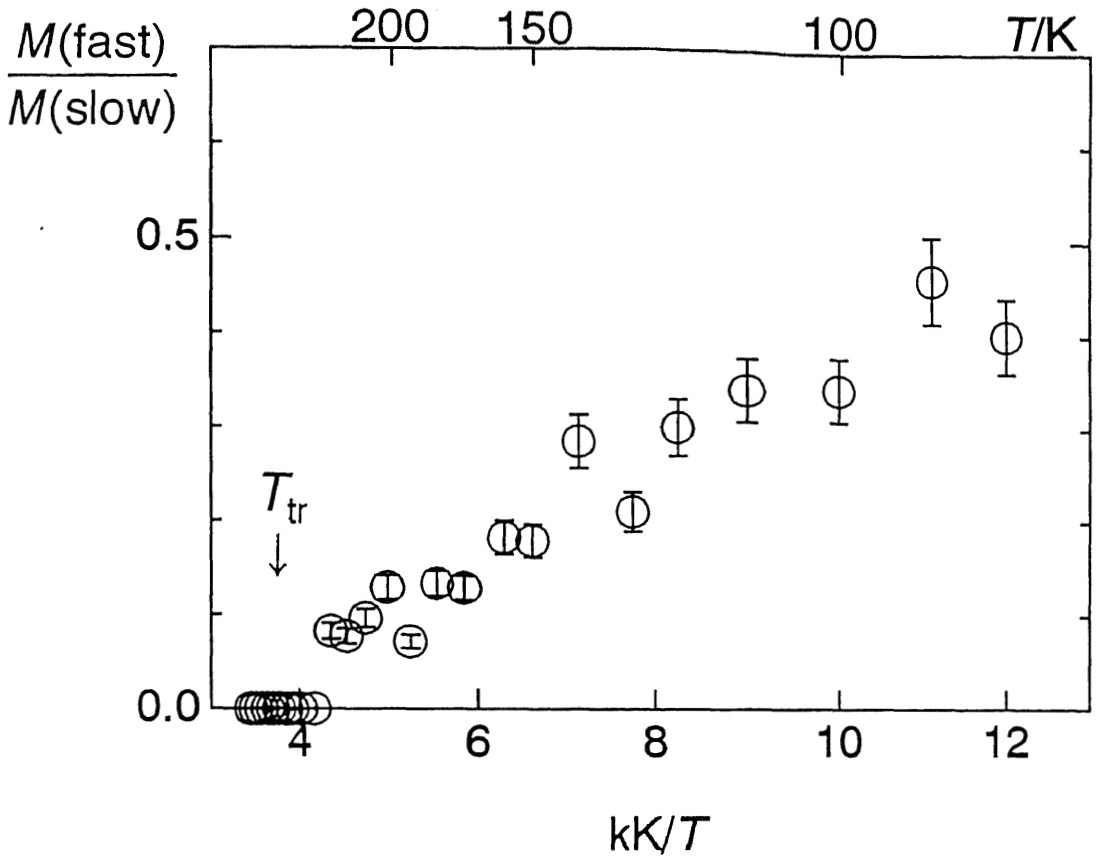

Fig. 2-17 A temperature dependence of the ^{1}H magnetization ratio, [M (fast) / M (slow)] of fast to slow recovering component observed at 54.25 MHz in $[Pd(en)_2][PdCl_2(en)_2](ClO_4)_4$. T_{tr} is the phase-transition temperature of 263 K determined by DSC measurement.

short component can be assigned to the relaxation due to trapped or fixed paramagnetic Pd^{3+} sites on the chain. This is because the magnitude of magnetic dipolar interactions between the paramagnetic impurities and protons located close to the electron spins depends upon the electron-proton distances.

On the other hand, the slow component with exponential behaviour is attributable to rapidly diffusing electron spins, which gives averaged fluctuation of magnetic field at protons located over a wide range along the chains. The observed gradual decrease of the fast component upon heating can be attributable to the onset of diffusion of the trapped spins by thermal excitation. In fact, the temperature dependence of T_1 given in Fig. 2-18 shows a gradual shortening of T_1 upon heating implying that the contribution from the diffusing spins to ^1H relaxation (slow component) increases with temperature.

The 1-D electron-spin diffusion can be investigated by measuring the Larmor-frequency dependence of T_1, as shown in Sections 2.3.1 and 2.3.2. T_1^{-1} versus $\omega^{-1/2}$ plots observed at two temperatures (90 and 140 K) are shown in Fig. 2-19. The clear $\omega^{1/2}$ dependence of the observed T_1 is explainable by the fluctuation of magnetic field made by electron spins randomly jumping along 1-D lattice proposed by Devreux *et al.* [39-41]. When the spin diffusion rate D^* on the chain fulfills $D^* \gg \omega_H$, ω_e, T_1 is satisfied with the relationship given by Eq. (2-12). In Eq. (2-12), the electron-spin susceptibility χ_s is roughly evaluated, as derived in Section 2.3.1, by assuming that

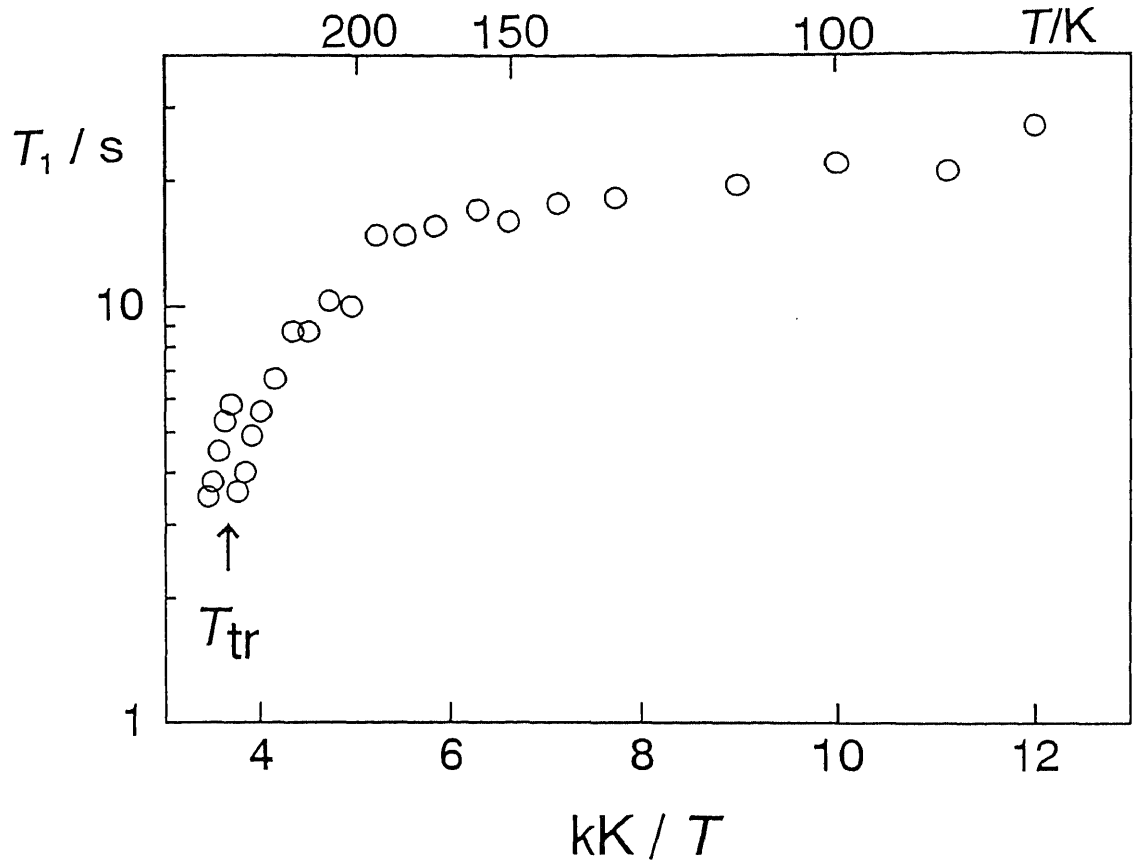

Fig. 2-18 A temperature dependence of ^1H T_1 observed at 54.25 MHz in $[Pd(en)_2][PdCl_2(en)_2](ClO_4)_4$. T_{tr} indicates the phase-transition temperature.

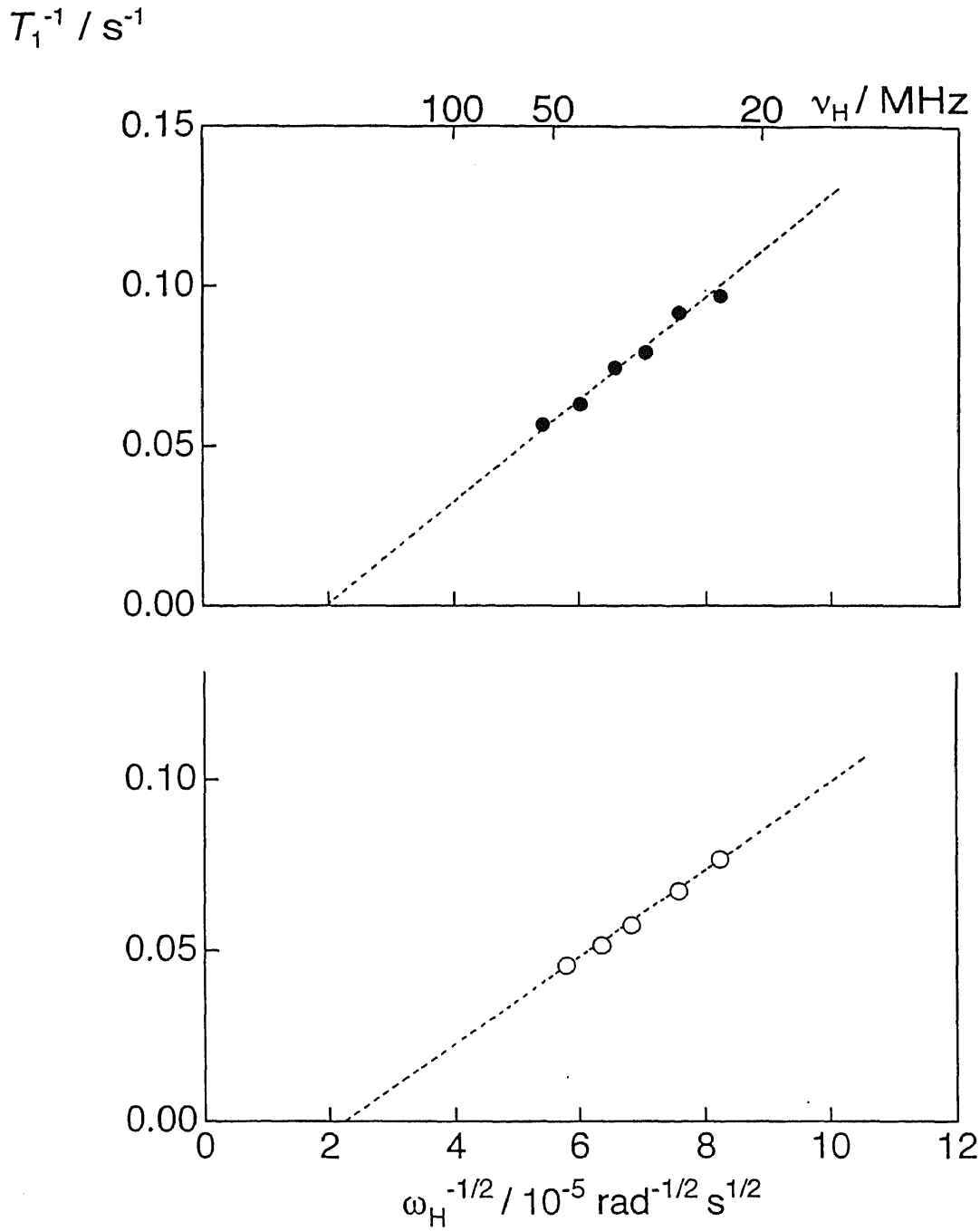

Fig. 2-19 Larmor-frequency (ω_H) dependences of T_1 of the slow relaxing components observed at 90 (○) and 140 K (●) in $[Pd(en)_2][PdCl_2(en)_2](ClO_4)_4$. Dotted lines are fitted theoretical values, proportional to the square root of the Larmor frequency ν_H (angular frequency ω_H).

temperature dependence of the concentration of the diffusing spins is proportional to that of the slow component presented in Fig. 2-17. Using this χ_s, and the d value of 4.5 $\times 10^{14}$ rad^4 s^{-2} which was derived from the reported crystal data [7], the temperature dependence of D^* is obtained as shown in Fig. 2-20. The high D^* values amounting to 10^{12} rad s^{-1} seem to be explained by the neutral solitons model because a very low electrical conductivity of 10^{-12} S cm^{-1} has been reported [42] at room temperature. This neutral soliton is expected to be produced by the phase mismatching of the Peierls distortion in the model shown in Fig. 2-9.

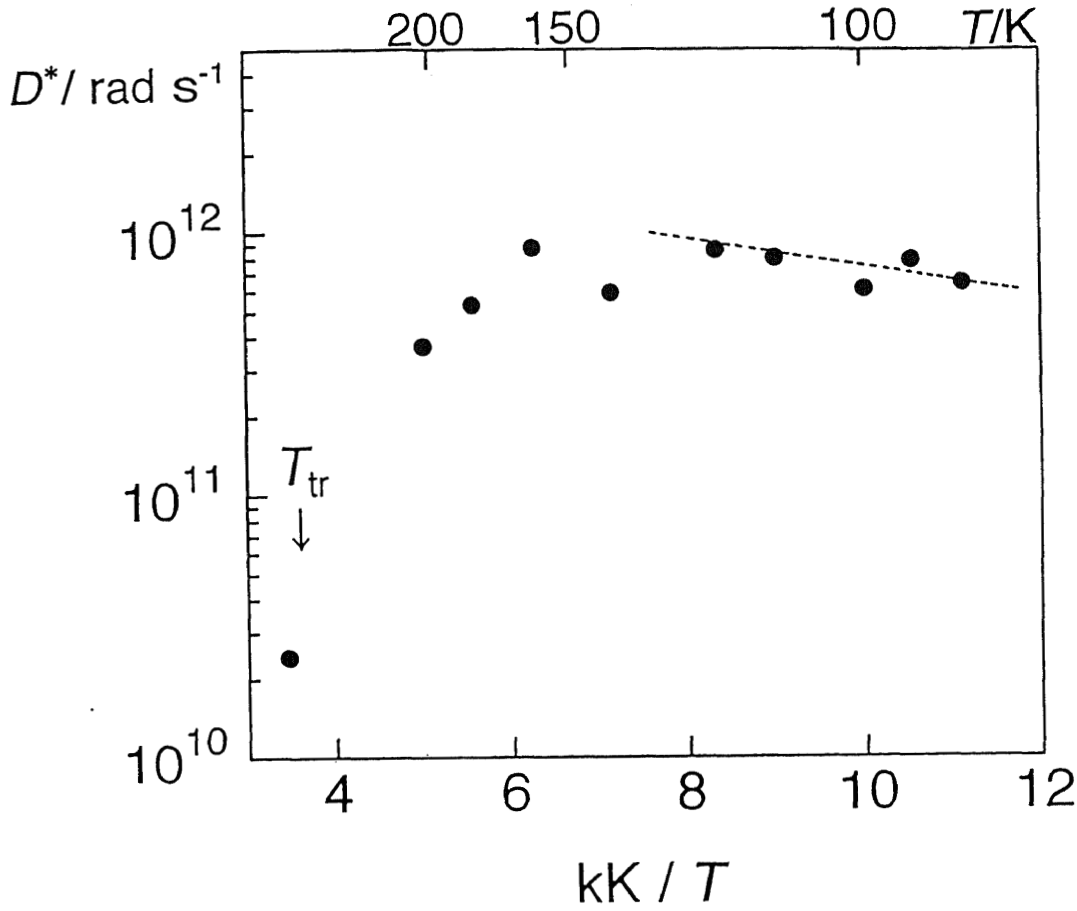

Fig. 2-20 The temperature dependence of 1-D diffusion rate D^* of electron spins determined in $[Pd(en)_2][PdCl_2(en)_2](ClO_4)_4$. The slope of the dotted line gives an activation energy of 11 ± 4 meV. T_{tr} indicates the phase-transition temperature.

2.3.4 $[Pd(en)_2][PtX_2(en)_2](ClO_4)_4$

In the foregoing discussion, we attributed the paramagnetic sites formed in $[M(en)_2][MX_2(en)_2](ClO_4)_4$ (M: Pt, Pd; X: Cl, Br) to neutral solitons. This explanation could not be directly derived from our experiments, but, as an alternative possibility, the model of polarons also can be applied to the above system. To confirm the formation of neutral solitons in $[Pt(en)_2][PtBr_2(en)_2](ClO_4)_4$ and $[Pd(en)_2][PdX_2(en)_2](ClO_4)_4$ (X: Cl, Br), electron spin behaviour in a hetero-metal complex $[Pd(en)_2][PtX_2(en)_2](ClO_4)_4$ (**1**) was investigated by measuring ESR, ^1H NMR T_1 and differential scanning calorimetry (DSC). The chain structure in the complex **1** is shown as $-Pd^{2+}$-X-Pt^{4+}-X- which has the non-degeneracy in the electronic ground state, which makes the solitons formation more difficult as mentioned in Section 2.1.

The ESR spectra of **1** observed in the temperature range of 150- 300 K revealed the presence of paramagnetic sites whose concentration was shown to have almost temperature independent values of *ca.* 10^{-5} in molar ratio to the normal Pd^{2+} and Pt^{4+} sites, and these values are one order of magnitude lower than those in $[M(en)_2][MX_2(en)_2](ClO_4)_4$ (X: Cl, Br) (**2**). With increasing temperature, the spectra showed no marked narrowing attributable to the electron-spin motion as observed in **2**.

The ^1H NMR T_1 measurement of **1** in the Larmor frequency and temperature ranges of 20- 54 MHz and 90- 320 K, respectively, afforded roughly exponential behaviour of the magnetization recovery. The T_1 values observed at 140 K

(54.3 MHz) in mixed metal complexes $[Pd(en)_2][PtCl_2(en)_2](ClO_4)_4$ and $[Pd(en)_2][PtBr_2(en)_2](ClO_4)_4$ were 77 and 74 s, respectively, which are much longer than 7.4 s in $[Pt(en)_2][PtBr_2(en)_2](ClO_4)_4$, 18.2 s in $[Pd(en)_2][PdBr_2(en)_2](ClO_4)_4$ and 17.6 s in $[Pd(en)_2][PdCl_2(en)_2](ClO_4)_4$.

The DSC measurement revealed phase transitions in chloro- and bromo-complexes at 281±1 and 295±1 K, respectively, with almost the same transition enthalpy of *ca.* 10 kJ mol^{-1}. Besides these anomalies, small heat absorptions were observed in bromo-complex at 275±5 and 300±3 K. Since these temperatures are close to those observed in **2**, the small anomalies are attributable to crystal **2** mixed in a small amount in the crystal **1**. The area ratio of **1** to **2** obtained in the DSC curves was *ca.* 10^{-2}.

The NMR relaxation-time measurement can afford a sensitive probe for detecting any unpaired spin located in the neighbourhood of resonant nuclei. The long ^1H T_1 in **1** implies the presence of a smaller amount of paramagnetic spins than in **2**. The exponential behaviour of the ^1H magnetization recovery and the quite long T_1 are mostly attributable to a nuclear spin-diffusion under a low concentration of the electron spins. The fact that the contribution to this mechanism from the fast component with distributed T_1 values as described in Sections 2.3.1, 2.3.2 and 2.3.3 was very small can be explained by the low spin density. By comparing the spin concentration derived from ESR spectra and ^1H magnetization recovery curves and T_1 values observed in **1** with

those in **2**, it is clear that paramagnetic M^{3+} sites become difficult to be formed in **1**. It is noted that **1** has a non-degenerate electronic ground state which makes the formation of neutral solitons difficult. On the other hand, $[Pt(en)_2][PtBr_2(en)_2](ClO_4)_4$ (see Section 2.3.1), $[Pd(en)_2][PdBr_2(en)_2](ClO_4)_4$ (see Section 2.3.2) and $[Pd(en)_2][PdCl_2(en)_2](ClO_4)_4$ (see Section 2.3.3) which have the twofold degeneracy of the chain structure have a higher concentration of electron spins which showed rapid 1-D spin diffusion. These results support our assignment that the diffusing spins observed in **2** form neutral solitons, in other words, the neutral-soliton concentration in **1** is quite low. From the analysis of DSC measurement, it seems that a part of a small amount of paramagnetic spins observed by ESR spectra in **1** is attributable to be neutral solitons formed in **2** mixing in a small amount in **1**.

2.3.5 Comparison of D^*

The evaluated diffusion rate D^* and the activation energy obtained on $[Pt(en)_2][PtBr_2(en)_2](ClO_4)_4$ and $[Pd(en)_2][PdX_2(en)_2](ClO_4)_4$ (X: Cl, Br) are in the order of 10^{12}- 10^{13} rad s^{-1} and 5- 20 meV, respectively, below *ca.*150 K, which are comparable to those reported in $[Pd(chxn)_2][PdBr_2(chxn)_2]Br_4$ and *trans*-polyacetylene as shown in Table 2-1. The D^* values of $[M(en)_2][MX_2(en)_2](ClO_4)_4$ and polyacetylene [46] are larger than 10^{12} rad s^{-1} [31] determined in $[Pd(chxn)_2][PdBr_2(chxn)_2]Br_4$ having a 2-D ordering structure of valence state. This difference can be explained by the marked isolated 1-D structure of $[M(en)_2][MX_2(en)_2](ClO_4)_4$ and polyacetylene favorable to the soliton diffusion. The difference of the D^* values between $[Pd(en)_2][PdCl_2(en)_2](ClO_4)_4$ and $[Pd(en)_2][PdBr_2(en)_2](ClO_4)_4$ in 90- 150 K is supported from the consideration of difference in the electron overlap between the Pd d_z^2 orbital and the halogen p_z orbital.

Table 2-1 The comparisons of the spin concentration (n) in molar ratio, the diffusion rate (D^* / rad s^{-1}), the activation energy (E_a / meV), the delocalization length (λ) of the electron spin diffusion in the temperature range 90- 150 K, the electrical conductivity (σ / S cm^{-1}) along the chain and the ratio (R) of the M^{4+}-X / M^{2+}-X bond lengths at room temperature evaluated in $[M(en)_2][MX_2(en)_2](ClO_4)_4$, $[Pd(chxn)_2][PdBr_2(chxn)_2]Br_4$ and *trans*-polyacetylene.

	n	D^* / rad s^{-1}	E_a / meV	λ	σ / S cm^{-1}	R
$[Pt(en)_2][PtBr_2(en)_2](ClO_4)_4$	10^{-4} [25]	$4\text{-}10\times10^{12}$	17	---	10^{-11} [42]	0.83 [13]
$[Pd(en)_2][PdBr_2(en)_2](ClO_4)_4$	10^{-4}	$1\text{-}3\times10^{13}$	7.5	15	10^{-8} [42]	0.86 [9]
$[Pd(en)_2][PdCl_2(en)_2](ClO_4)_4$	10^{-4}-10^{-5}	$6\text{-}10\times10^{12}$	11	---	10^{-12} [42]	0.77 [7]
$[Pd(chxn)_2][PdBr_2(chxn)_2]Br_4$	3×10^{-3} [10]	10^{12} [31]	2-8 [31]	20 [31]	10^{-3} [31]	0.91 [10]
trans-polyacetylene	10^{-3}-10^{-4} [46]	$2\text{-}4\times10^{13}$ [46]	---	17 [46]	10^{-5} [50]	---

2.4 Conclusion

^{1}H NMR relaxation measured on $[Pt(en)_2][PtBr_2(en)_2](ClO_4)_4$ and $[Pd(en)_2][PdX_2(en)_2](ClO_4)_4$(X: Cl, Br) containing the almost isolated 1-D structure showed marked influences from the paramagnetic spins which rapidly diffuse with a small activation energy even at temperatures below *ca.*150K. The observed Larmor-frequency dependence of ^{1}H T_1 can be explained well by the Devreux's treatment of 1-D spin diffusion with delocalized spins along the chain. This spin motion is attributable to neutral solitons by referring to the data of the electrical conductivity and comparing the ESR and NMR data of mixed metal complexes $[Pd(en)_2][PtX_2(en)_2](ClO_4)_4$ (X: Cl, Br) with the non-degenerate ground state. The evaluated diffusion rate D^* and the activation energy are in the order of 10^{12}-10^{13} rad s^{-1} and 5-20 meV, respectively, below *ca.* 150K, which are comparable to those reported in $[Pd(chxn)_2][PdBr_2(chxn)_2]Br_4$ and *trans*-polyacetylene.

References to Chapter 2

1. N. Matsumoto, M. Yamashita and S. Kida, *Bull. Chem. Soc. Jpn.*, **51**, 2334 (1978).
2. N. Matsumoto, M. Yamashita and S. Kida, *Bull. Chem. Soc. Jpn.*, **51**, 3514 (1978).
3. M. Yamashita, N. Matsumoto and S. Kida, *Inorg. Chim. Acta*, **31**, L381 (1978).
4. N. Matsumoto, M. Yamashita, S. Kida and I. Ueda, *Acta Crystallogr.*, **B35**, 1458 (1979).
5. H. Endres, H.J. Keller, R. Martin, H.N. Gung and U. Traeger, *Acta Crystallogr.*, **B35**, 1885 (1979).
6. H. Endres, H.J. Keller, R. Martin, U. Traeger and M. Novotny, *Acta Crystallogr.*, **B36**, 35 (1980).
7. A.L. Beauchamp, D. Layek and T. Theophanides, *Acta Crystallogr.*, **B38**, 1158 (1982).
8. M. Yamashita, H. Ito, K. Toriumi and T. Ito, *Inorg. Chem.*, **22**, 1566 (1983).
9. M. Yamashita, K. Toriumi and T. Ito, *Acta Crystallogr.*, **C41**, 876 (1985).
10. H. Okamoto, K. Toriumi, T. Mitani and M. Yamashita, *Phys. Rev.*, **B42**, 10381 (1990).
11. J.B. Weinrach, S.A. Ekberg, S.D. Conradson, B.I. Swanson and H.D. Hochheimer, *Inorg. Chem.*, **29**, 981 (1990).
12. S.C. Huckett, B. Scott, S.P. Love, R.J. Donohoe, C.J. Burns, E. Garcia, T.

Frankcom and B.I. Swanson, *Inorg. Chem.*, **32**, 2137 (1993).

13. K. Toriumi, M. Yamashita, S. Kurita, I. Murase and T. Ito, *Acta Crystallogr.*, **B49**, 497 (1993).
14. J.F. Bardeau, A. Bulou, W.T. Klooster, T.F. Koetzle, S. Johnson, B. Scott, B.I. Swanson and J. Eckert, *Acta Crystallogr.*, **B52**, 854 (1996).
15. G.F. Strouse, B. Scott, M. Berkey, S. Johnson, T. Darling, A. Migliori and B.I. Swanson, *Synth. Metals*, **86**, 1919 (1997).
16. R.J.H. Clark, M. Kurmoo, D.N. Mountney and H. Toftlund, *J. Chem. Soc. Dalton Trans.*, 1851 (1982).
17. R.J.H. Clark and M. Kurmoo, *J. Chem. Soc. Faraday Trans. 2*, **79**, 519 (1983).
18. Y. Wada, T. Mitani, M. Yamashita and T. Koda, *J. Phys. Soc. Jpn.*, **54**, 3143 (1985).
19. H. Toftlund, P.W. Jensen and C.S. Jacobsen, *Chem. Phys. Lett.*, **142**, 286 (1987).
20. K. Okaniwa, H. Okamoto, T. Mitani, K. Toriumi and M. Yamashita, *J. Phys. Soc. Jpn.*, **60**, 997 (1991).
21. H. Okamoto and T. Mitani, *Prog. Theor. Phys.*, **113**, 191 (1993).
22. A. Girlando, A. Painelli, M. Ardoino and C. Bellitto, *Phys. Rev.*, **51**, 17338 (1995).
23. H. Okamoto, Y. Oka, T. Mitani and M. Yamashita, *Phys. Rev.*, **55**, 6330 (1997).
24. R. Aoki, Y. Hamaue, S. Kida, M. Yamashita, T. Takemura, Y. Furuta and A. Kawamori, *Mol. Cryst. Liq. Cryst.*, **81**, 301 (1982).

25. A. Kawamori, R. Aoki and M. Yamashita, *J. Phys.C*, **18**, 5487 (1985).

26. M. Haruki and S. Kurita, *Phys. Rev.*, **39**, 5706 (1989).

27. R. Ikeda, T. Tamura and M. Yamashita, *Chem. Phys. Lett.*, **173**, 466 (1990).

28. C.A. Arrington, C.J. Unkefer, R.J. Donohoe, S.C. Huckett, S. Kurita and B.I. Swanson, *Solid State Commun.*, **84**, 979 (1992).

29. H. Okamoto, K. Toriumi, T. Mitani and M. Yamashita, *Mol. Cryst. Liq. Cryst.*, **218**, 247 (1992).

30. R. Ikeda, A. Ghosh, L.S. Prabhumirashi, D. Nakamura and M. Yamashita, *Mol. Cryst. Liq. Cryst.*, **216**, 181 (1992).

31. R. Ikeda, M. Iida, T. Asaji, A. Ghosh and M. Yamashita, *Chem. Phys. Lett.*, **210**, 78 (1993).

32. S. Ichinose, *Solid State Commun.*, **50**, 137 (1984).

33. Y. Onodera, *J. Phys. Soc. Jpn.*, **56**, 250 (1987).

34. M. Yamashita, I. Murase, T. Ito, Y. Wada, T. Mitani and I. Ikemoto, *Bull. Chem. Soc. Jpn.*, **58**, 2336 (1985).

35. K. Toriumi, M. Yamashita and I. Murase, *Chem. Lett.*, 1753 (1986).

36. Y. Wada, T. Mitani, K. Toriumi and M. Yamashita, *J. Phys. Soc. Jpn.*, **58**, 3013 (1989).

37. M. Sakai, M. Hayakawa, N. Kuroda, Y. Nishina and M. Yamashita, *J. Phys. Soc. Jpn.*, **60**, 1619 (1991).

38. W.E. Blumberg, *Phys. Rev.*, **119**, 79 (1960).

39. F. Devreux, J.-P. Boucher and M. Nechtschein, *J. Phys.* (Paris), **35**, 271 (1974).

40. F. Devreux and M. Nechtschein, in *Lectures Notes in Physics*, ed. by S. Barisic, A. Bjelis, J.R. Cooper and B. Leontic (Springer, Berlin, 1979) p145.

41. F. Devreux, *Phys. Rev.*, **B25**, 6609 (1982).

42. Y. Hamaue, R. Aoki, M. Yamashita and S. Kida, *Inorg. Chim. Acta*, **54**, L13 (1981).

43. K. Compaan and Y. Haven, *Trans. Faraday Soc.*, **52**, 786 (1956).

44. W. Smith and M.J. Gillan, *Ber. Bunsenges. Physik. Chem.*, **95**, 967 (1991).

45. H. Ibach and H. Lüth, *Festkörperphysik* (Springer, Berlin, 1981) p219.

46. M. Nechtstein, F. Devreux, F. Genoud, M. Guglielmi and K. Holczer, *Phys. Rev.*, **B27**, 61 (1983).

47. A. Mishima and K. Nasu, *Phys. Rev.*, **B39**, 5758 (1989).

48. A. Mishima and K. Nasu, *Phys. Rev.*, **B39**, 5763 (1989).

49. M. Suzuki and K. Nasu, *Phys. Rev.*, **B45**, 1605 (1992).

50. H. Shirakawa, T. Ito and S. Ikeda, *Polym. J.*, **4**, 460 (1973).

Chapter 3

Valence Structure of Halogen-Bridged -Pt-Pt-X-Pt-Pt-X- Type Complexes

3.1 Introduction

Recently, a new halogen-bridged one-dimensional (1-D) system, $[Pt_2X(P_2O_5H_2)_4]^{4-}$ (X: Cl, Br, I), consisting of -Pt-Pt-X-Pt-Pt-X- type chains has been prepared [1-5]. Two Pt atoms are surrounded by four diphosphite ligands which bridge two Pt atoms as shown in Fig. 3-1 [1-4]. In this system, new properties different from those in the $-M^{2+}-X-M^{4+}-X-$ type complexes can be expected, because of the presence of metal-metal bonds. In fact, $K_4[Pt_2X(P_2O_5H_2)_4]$ (X: Cl, Br, I) have been reported to have electrical conductivities of *ca.* 10^{-6}, 10^{-3} and 10^{-1} S cm^{-1} [1-3] in chloro-, bromo- and iodo-complexes, respectively, around room temperature. These values are much higher than 10^{-8} - 10^{-15} S cm^{-1} observed in $-Pt^{2+}-X-Pt^{4+}-X-$ complexes [6].

Possible models of the Pt valence state in $[Pt_2X(P_2O_5H_2)_4]^{4-}$ can be proposed to be

(A) $-Pt^{2+}-Pt^{2+}-X-Pt^{3+}-Pt^{3+}-X-$,

(B) $-Pt^{2+}-Pt^{3+}-X-Pt^{2+}-Pt^{2+}-X-$,

(C) $-Pt^{2+}-Pt^{3+}-X-Pt^{3+}-Pt^{2+}-X-$,

and

(D) $-Pt^{2.5+}-Pt^{2.5+}-X-$.

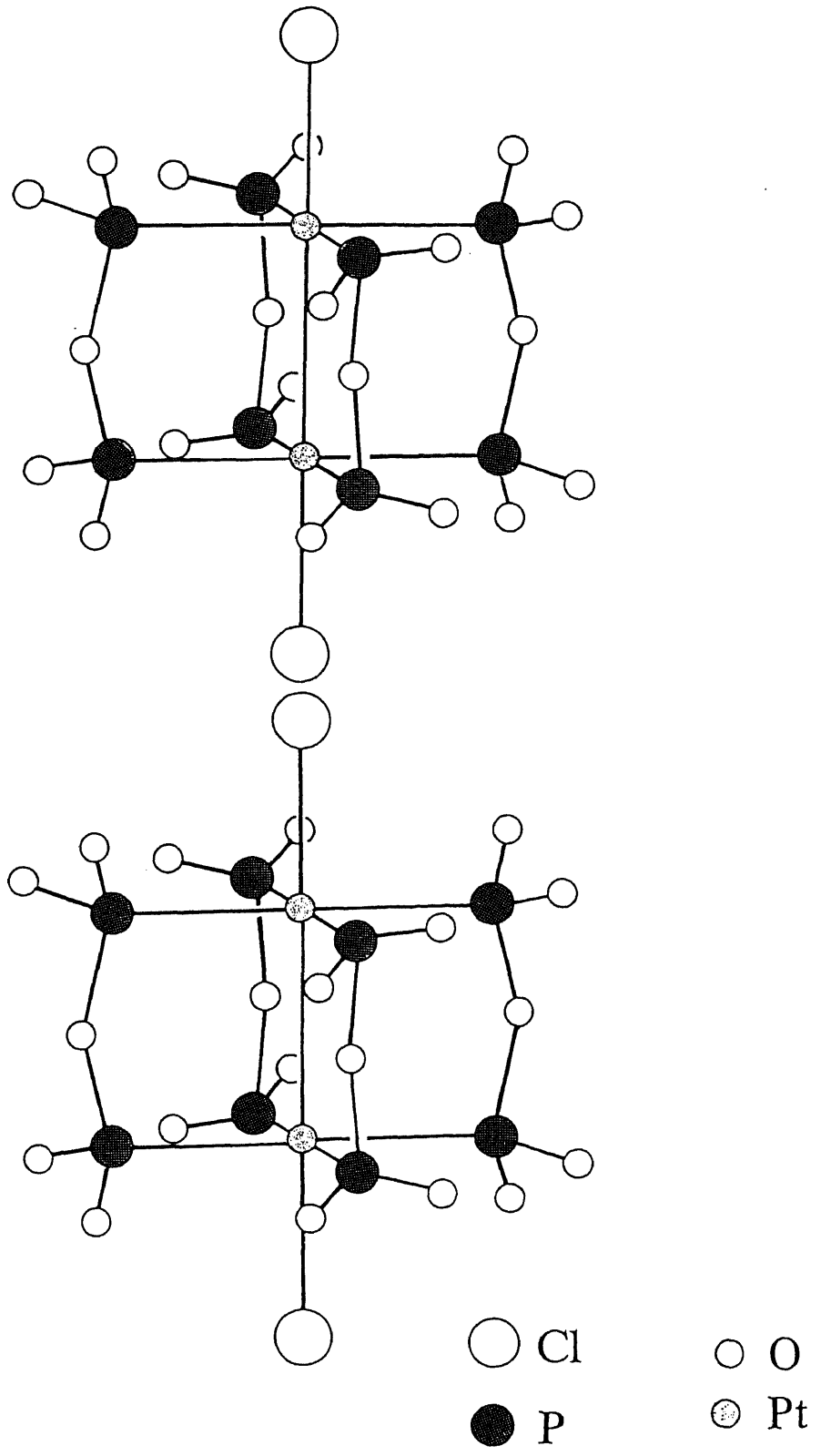

Fig. 3-1 The structure of a one-dimensional polymer complex, $(NH_4)_4[Pt_2Cl(P_2O_5H_2)_4]$ determined by the X-ray diffraction [4]. Only atomic arrangements in the anions are shown. The positions of the bridged chlorine atoms are disordered over two sites in the chain.

The probable valence structures have been discussed based on the studies of X-ray diffraction [1-5], magnetic susceptibility [3] and electronic and vibrational spectra [7]. No consistent conclusion on the valence structure could not be derived from the respective methods.

In this study, it is intended to obtain the accurate information on the Pt valence state in the 1-D complexes $(NH_4)_4[Pt_2X(P_2O_5H_2)_4]$ by observing the ^{31}P NMR chemical shift in the ligand atoms which is sensitive to the local electronic distribution around nuclei. To measure the chemical shift in solid state, the magic angle spinning (MAS) NMR technique was applied.

3.2 Experimental

Sample Preparation

3.2.1 Binuclear Pt^{2+} Monomer Complexes

A Pt^{2+} monomer complex, $K_4[Pt_2(P_2O_5H_2)_4]\cdot 2H_2O$ was synthesized by the reported method [1,8,9] and used as the starting material for the preparation of Pt^{3+} monomer and polymer complexes. Since this Pt^{2+} potassium salt is air sensitive and gradually decomposes in air, a stable Pt^{2+} monomer, $Ba_2[Pt_2(P_2O_5H_2)_4]$ was prepared at the same time according to literature [9]. Both complexes were used for the NMR measurement.

3.2.2 Binuclear Pt^{3+} Monomer Complexes

Pt^{3+} monomer complexes, $K_4[Pt_2X_2(P_2O_5H_2)_4]\cdot 2H_2O$ (X: Cl, Br) were prepared according to the reported method [3,7]. The complex of $K_4[Pt_2I_2(P_2O_5H_2)_4]\cdot nH_2O$ was prepared by adding I_2 in a solution of Pt^{2+} potassium salt dissolved in CH_3OH+H_2O (1:1) followed by evaporation of solvent to dryness. Excess I_2 remaining in the crystals was removed by washing with ether.

3.2.3 One-Dimensional Polymer Pt-Complexes

Polymer complexes, $(NH_4)_4[Pt_2X(P_2O_5H_2)_4]$ (X: Cl, Br) were synthesized according to the reported method [1-3]. $(NH_4)_4[Pt_2I(P_2O_5H_2)_4]$ was prepared in a similar

manner to chloro- and bromo-complexes.

To identify the obtained crystals, X-ray powder patterns were measured by use of a Rigaku CN2155D5 goniometer operating at 30kV and 10-15mA, and graphitemonochromated Cu Kα radiation at room temperature. The obtained patterns were compared with the reported data [1-4].

Solid State NMR

A Bruker MSL-300 spectrometer equipped with a Bruker CP / MAS probe head with a 5mm rotor was used for the measurement of ^{31}P NMR spectra at a Larmor frequency of 121.496 MHz and at room temperature. A spinning rate of *ca.* 5 kHz was employed and 8 scans were accumulated for each spectrum. An 85% aqueous solution of H_3PO_4 was used as the external standard of chemical shift. Since the shift value of PO_4^{3-} ions present as an impurity in the samples coincided with this standard shift value, this PO_4^{3-} signal was used as the internal standard. The ^{31}P spin-lattice relaxation time T_1 was measured between 290 and 360 K using the saturation recovery method.

3.3 Results and Discussion

3.3.1 Binuclear Pt^{2+} Monomer Complexes

The observed ^{31}P NMR spectra of Pt^{2+} monomers, $K_4[Pt_2(P_2O_5H_2)_4] \cdot 2H_2O$ and $Ba_2[Pt_2(P_2O_5H_2)_4]$ at room temperature are shown in Fig. 3-2. A single ^{31}P line is observed for both complexes with satellites due to the coupling between ^{31}P and ^{195}Pt (I=1/2, natural abundance 33.8%), indicating direct P - Pt bonding. The determined values of the chemical shifts (δ) and coupling constants (J) are listed in Table 3-1. These observed values agree well with δ=66.14 ppm and J=3.073 kHz reported for $K_4[Pt_2(P_2O_5H_2)_4]$ in an aqueous solution [9].

3.3.2 Binuclear Pt^{3+} Monomer Complexes

The spectra observed in Pt^{3+} monomer complexes, $K_4[Pt_2X_2(P_2O_5H_2)_4] \cdot 2H_2O$ (X: Cl, Br) and $K_4[Pt_2I_2(P_2O_5H_2)_4] \cdot nH_2O$, are shown in Fig. 3-3. Bromo- and iodo- complexes yielded a single line with a pair of satellites in agreement with the X-ray structural study [2] reporting the equivalence of all P atoms in crystal. On the other hand, chloro-complex, reported to have four kinds of P sites in the crystal [1], gave a complex spectrum which could be shown to consist of four peaks corresponding to the nonequivalent P atoms by observing spectra at various spinning rates. The ^{31}P chemical shifts of these complexes shown in Table 3-1 are close to the reported values in aqueous solutions, *i.e.* 27.96, 24.01 and 18.01 ppm in chloro-, bromo- and iodo-complexes,

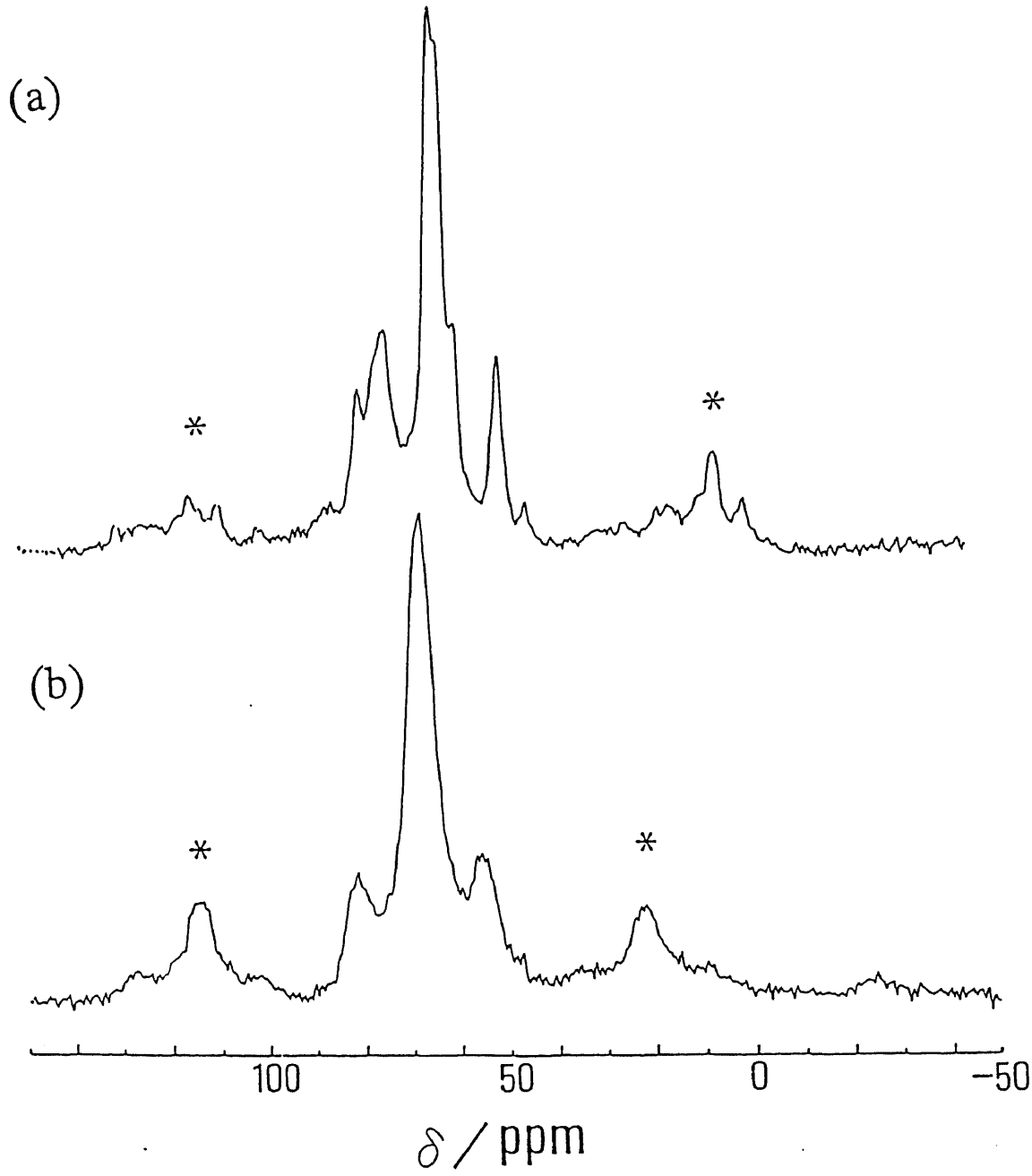

Fig. 3-2 ^{31}P MAS NMR spectra of monomer Pt^{2+} complexes: (a) $K_4[Pt_2(P_2O_5H_2)_4]\cdot 2H_2O$ and (b) $Ba_2[Pt_2(P_2O_5H_2)_4]$. Satellite lines of about one-third of the total intensity observed on both sides of the peak are formed by coupling between ^{31}P and ^{195}Pt with I=1/2 and 33.8% naturally abundant. The peaks with asterisks are spinning sidebands.

Table 3-1 ^{31}P chemical shifts (δ) and coupling constants ($J_{Pt\text{-}P}$) in binuclear Pt^{2+} and Pt^{3+} and polymer complexes observed by MAS NMR spectra at room temperature. The shift values were measured from an 85% aqueous H_3PO_4.

	compound	δ / ppm	$J_{Pt\text{-}P}$ / kHz
Pt^{2+}	$K_4[Pt_2(P_2O_5H_2)_4]$	65±2.0	3.4±0.1
	$Ba_2[Pt_2(P_2O_5H_2)_4]$	66±2.0	3.2±0.5
Pt^{3+}	$K_4[Pt_2Cl_2(P_2O_5H_2)_4]$	12±0.6 15±0.9 17±0.8 24±1.0	
	$K_4[Pt_2Br_2(P_2O_5H_2)_4]$	27±3.0	2.2±0.3
	$K_4[Pt_2I_2(P_2O_5H_2)_4]$	21±2.5	2.2±0.5
polymer	$(NH_4)_4[Pt_2Cl(P_2O_5H_2)_4]$	27±4.6 59±2.2 38±1.8 70±3.0	
	$(NH_4)_4[Pt_2Br(P_2O_5H_2)_4]$	24±3.5 53±1.5 36±1.5 65±2.0	
	$(NH_4)_4[Pt_2I(P_2O_5H_2)_4]$	19±2.6 65±1.7	2.3±0.5 2.5±0.5

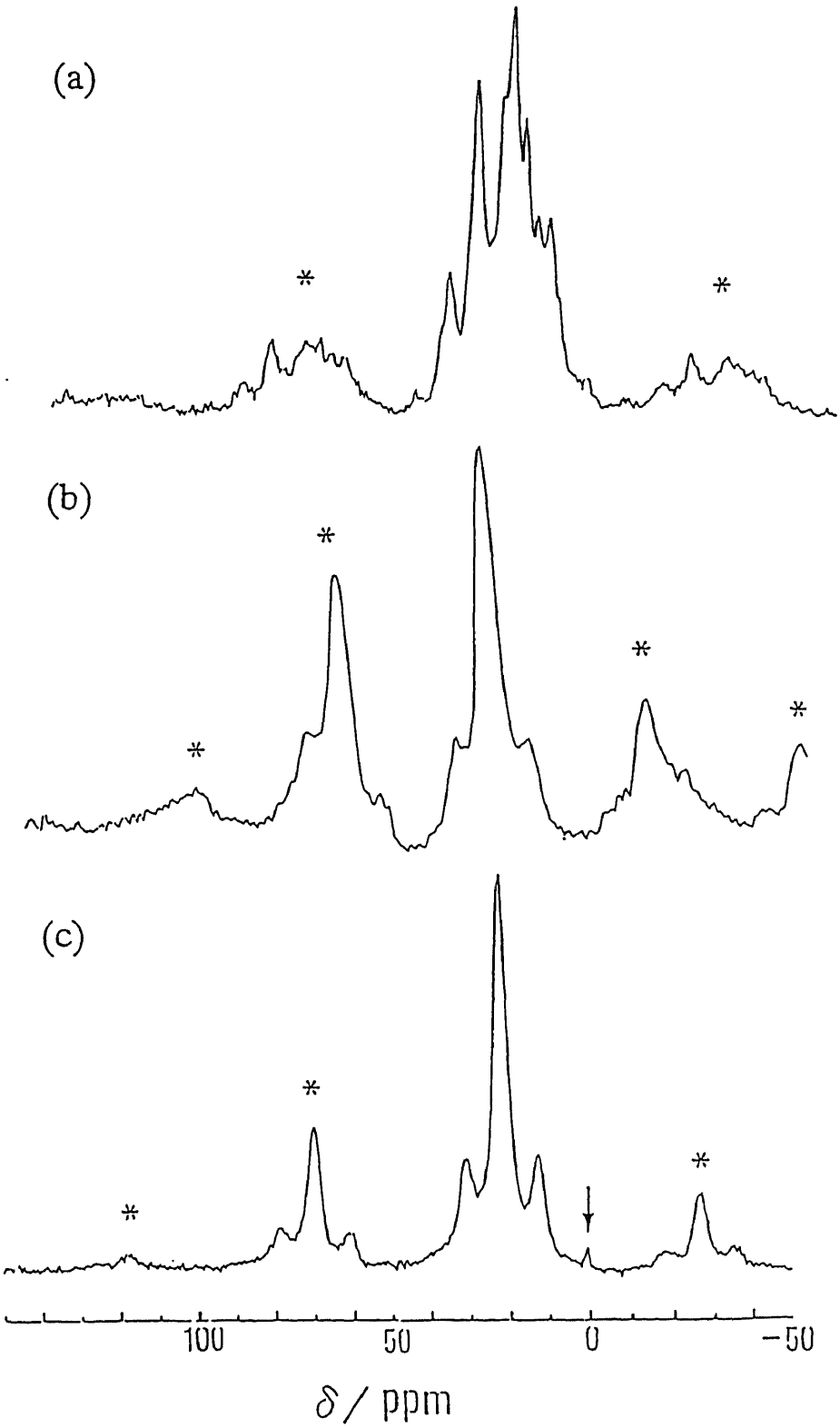

Fig. 3-3 ^{31}P MAS NMR spectra of monomer Pt^{3+} complexes: (a) $K_4[Pt_2Cl_2(P_2O_5H_2)_4]$ $\cdot 2H_2O$, (b) $K_4[Pt_2Br_2(P_2O_5H_2)_4]\cdot 2H_2O$, (c) $K_4[Pt_2I_2(P_2O_5H_2)_4]\cdot nH_2O$. The peaks with asterisks are spinning sidebands. The arrow shows the signal of PO_4^{3-} impurity which was used as the internal standard.

respectively [9-11]. The coupling constants $J_{Pt\text{-}P}$ given in Table 3-1 are also close to the reported values 2.100 and 2.139 kHz in bromo- and iodo- complexes, respectively, observed in aqueous solution [9-11]. These results for the Pt^{2+} and Pt^{3+} monomers imply that the structure of the complexes in solid is close to those in aqueous solution, namely, the presence of the almost isolated monomer complex ions is also expected in the solid state.

The ^{31}P chemical shift values in the Pt^{3+} complexes smaller than those in the Pt^{2+} complexes can be attributed to the difference in the paramagnetic shift δ_P which is inversely proportional to the electronic excitation energy associated with the ^{31}P valence electrons [12]. Spectroscopic studies on $K_4[Pt_2Cl_2(P_2O_5H_2)_4]$ and $K_4[Pt_2(P_2O_5H_2)_4]$ in solution [8,9] have shown that the electronic excitation energy in the Pt^{3+} complex is higher than that of the Pt^{2+} complex, consistent with the present tendency of chemical shift.

On chloro-, bromo- and iodo-complexes of Pt^{3+} in solution, the reported values of chemical shift [9-11], which increase in the order of I< Br< Cl, can also be qualitatively explained by the opposite order (Cl< Br< I) of energy differences of the reported electronic state [7, 8]. As for the solid state shift in the present Pt^{3+} complexes, this order can be applied except for the chloro-complex which exhibited multiple lines due to the low-symmetric crystal field.

It has been reported [13] that the coupling constant J decreases with the

increase in the coordination number of the coupled metal. The present result that four-coordinated Pt^{2+} complexes have J values larger than those in the six-coordinated Pt^{3+} system can be explained by this general trend.

It can be seen from Table 3-1 that the difference in the ^{31}P chemical shifts between Pt^{2+} and Pt^{3+} complexes (12- 27 and *ca.* 65 ppm, respectively) seems sufficiently large compared with the crystal field splittings of *ca.* 12 ppm as observed in Pt^{2+} chloro-complex. This result means that, from the NMR chemical shift measurement, it is possible to distinguish Pt^{2+} from Pt^{3+} and determine the Pt valence in the polymer complexes.

3.3.3 One-Dimensional Polymer Pt-Complexes

In Fig. 3-4, the ^{31}P NMR spectra observed in the polymer complexes $(NH_4)_4[Pt_2X(P_2O_5H_2)_4]$ (X: Cl, Br, I) are shown. Chloro- and bromo-complexes exhibited a pair of peaks with almost the equal intensity, and the observed shift values shown in Table 3-1 are close to those in the Pt^{2+} and Pt^{3+} monomers. X-ray structural studies on these complexes [4] revealed that there are two kinds of nonequivalent P sites in each $Pt_2(P_2O_5H_2)_4$ unit shown in Fig. 3-1. The respective doublet lines in Fig. 3-4, each of which was separated by *ca.* 10 ppm, can therefore be assigned to the two kinds of P atoms placed in different crystal fields. Since the averaged shift values for these doublets correspond to those in Pt^{2+} and Pt^{3+} monomers, the doublets observed at a high

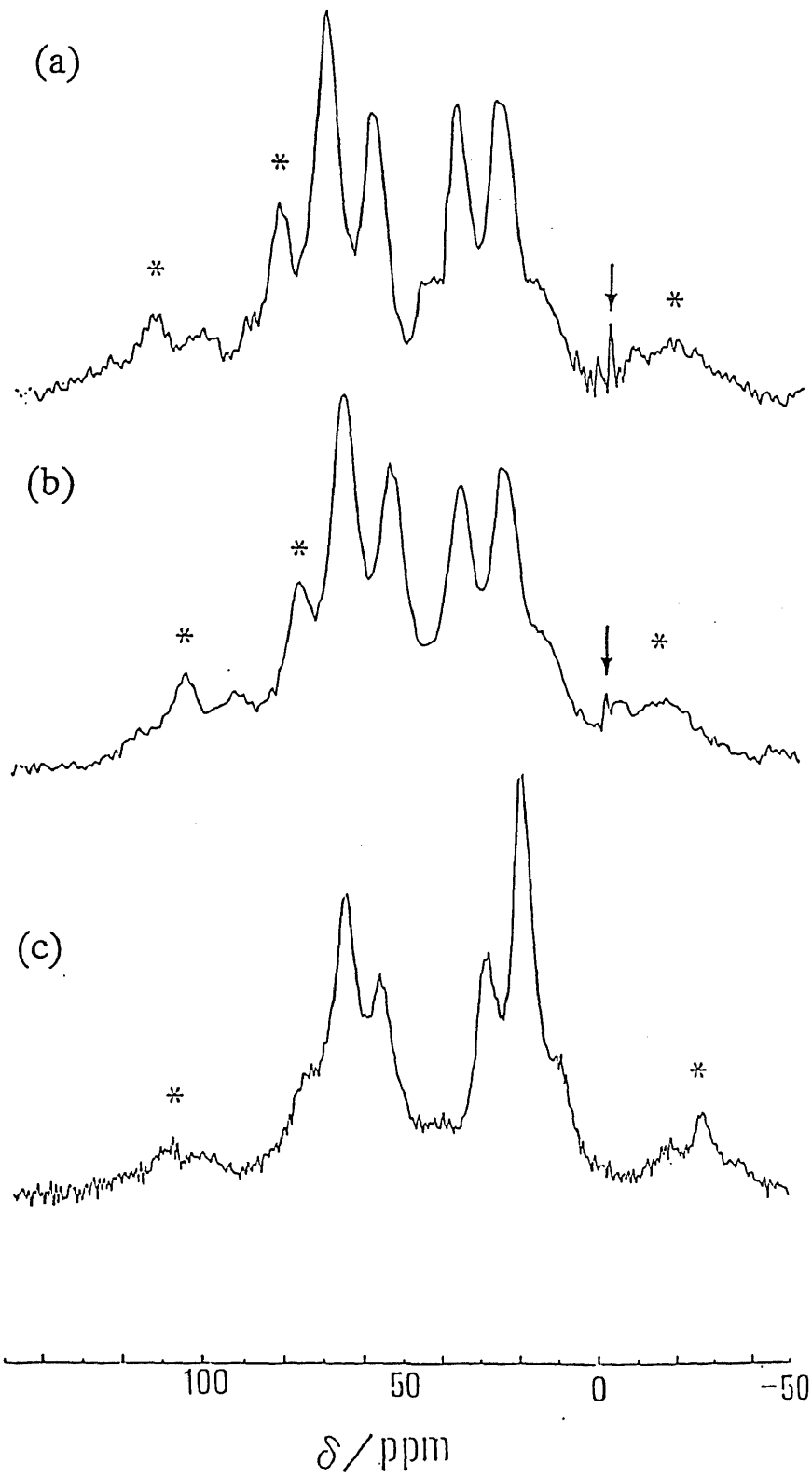

Fig. 3-4 ^{31}P MAS NMR spectra of polymer complexes: (a) $(NH_4)_4[Pt_2Cl(P_2O_5H_2)_4]$, (b) $(NH_4)_4[Pt_2Br(P_2O_5H_2)_4]$, (c) $(NH_4)_4[Pt_2I(P_2O_5H_2)_4]$. The peaks with asterisks are spinning sidebands. The arrows show the signal of PO_4^{3-} impurity which was used as the internal standard.

and a low field are attributable to the ^{31}P nuclei bonded to Pt atoms which are nearly di- and tri-valent, respectively. On the other hand, in iodo-complex, two peaks of roughly equal intensity were observed at 19 ± 2.6 and 65 ± 1.7 ppm also assignable to Pt^{2+} and Pt^{3+} states, respectively. These results clearly indicate that the present polymer complexes have a mixed valence structure in which the Pt atoms consist of two kinds of valence states close to Pt^{2+} and Pt^{3+} with almost the same concentration. The present NMR results, according, exclude the possibility of model (D) $-Pt^{2.5+}-Pt^{2.5+}-X-$ given above and supports models (A) $-Pt^{2+}-Pt^{2+}-X-Pt^{3+}-Pt^{3+}-X-$, (B) $-Pt^{2+}-Pt^{3+}-X-Pt^{2+}-Pt^{3+}-X-$ and (C) $-Pt^{2+}-Pt^{3+}-X-Pt^{3+}-Pt^{2+}-X-$.

In $(NH_4)_4[Pt_2I(P_2O_5H_2)_4]$, the ^{31}P-^{195}Pt coupling constant J could be determined as 2.3 ± 0.5 and 2.5 ± 0.5 kHz for ^{31}P coordinated to Pt^{3+} and Pt^{2+} atoms, respectively. Compared these J values with 3.4 and 3.2 kHz observed in solid state on monomer $K_4[Pt_2(P_2O_5H_2)_4]$ and $Ba_2[Pt_2(P_2O_5H_2)_4]$, respectively, the smaller value of 2.5 kHz in the polymer can be explained by the change of Pt^{2+} coordination after polymerization, namely, the Pt^{2+} coordination is no longer planar but close to octahedral, as seen in Fig.3-1.

In structure (A), Pt *d* electrons can be paired and no paramagnetic behaviour is expected, whereas an unpaired electron should be present at each unit in models (B) and (C). In (B) and (C) states, the fluctuation of magnetic field made by the paramagnetic spins at the position of ^{31}P nuclei gives strong influence on the ^{31}P spin-

lattice relaxation, although the unpaired spin in each unit is probably partly cancelled by the antiferromagnetic interaction with the neighbouring spins in the 1-D chain. On the other hand, no paramagnetic effect takes place in model (A). In fact, the Pt^{2+} and Pt^{3+} monomers with no paramagnetic spins showed quite long ^{31}P spin-lattice relaxation time T_1 amounting to *ca.* 100 and 40 s in $Ba_2[Pt_2(P_2O_5H_2)_4]$ and $K_4[Pt_2I_2(P_2O_5H_2)_4]$, respectively, at room temperature. The ^{31}P T_1 of the absorption lines at 19 and 65 ppm, observed in the polymer $(NH_4)_4[Pt_2I(P_2O_5H_2)_4]$ was measured by employing the saturation recovery method in the range 293-360 K. The magnetization recovery after a $\pi/2$ pulse was quite analogous for both lines and could not be expressed by a single exponential function as shown in Figs. 3-5 and 3-6 respectively, but it was fitted roughly by the sum of two T_1 values of 0.5 ± 0.2 and 100 ± 20 s for both lines in the temperature range studied. From the fact that the T_1 value of the slow recovery component which was in the majority (60- 80 %) of ^{31}P magnetization corresponds to those in the diamagnetic monomer complexes, the polymer complex $(NH_4)_4[Pt_2I(P_2O_5H_2)_4]$ is expected to have an intrinsically long T_1 indicating to be essentially diamagnetic. The observed T_1 values of the slow component in $(NH_4)_4[Pt_2Cl(P_2O_5H_2)_4]$ and $(NH_4)_4[Pt_2Br(P_2O_5H_2)_4]$ were also in the long range of 10- 100 s, and these complexes can be supposed to be in the diamagnetic state. This result cannot be explained by models (B) and (C), and hence model (A) is concluded to be the most probable. The presence of a fast (minor) magnetization component implies the formation of

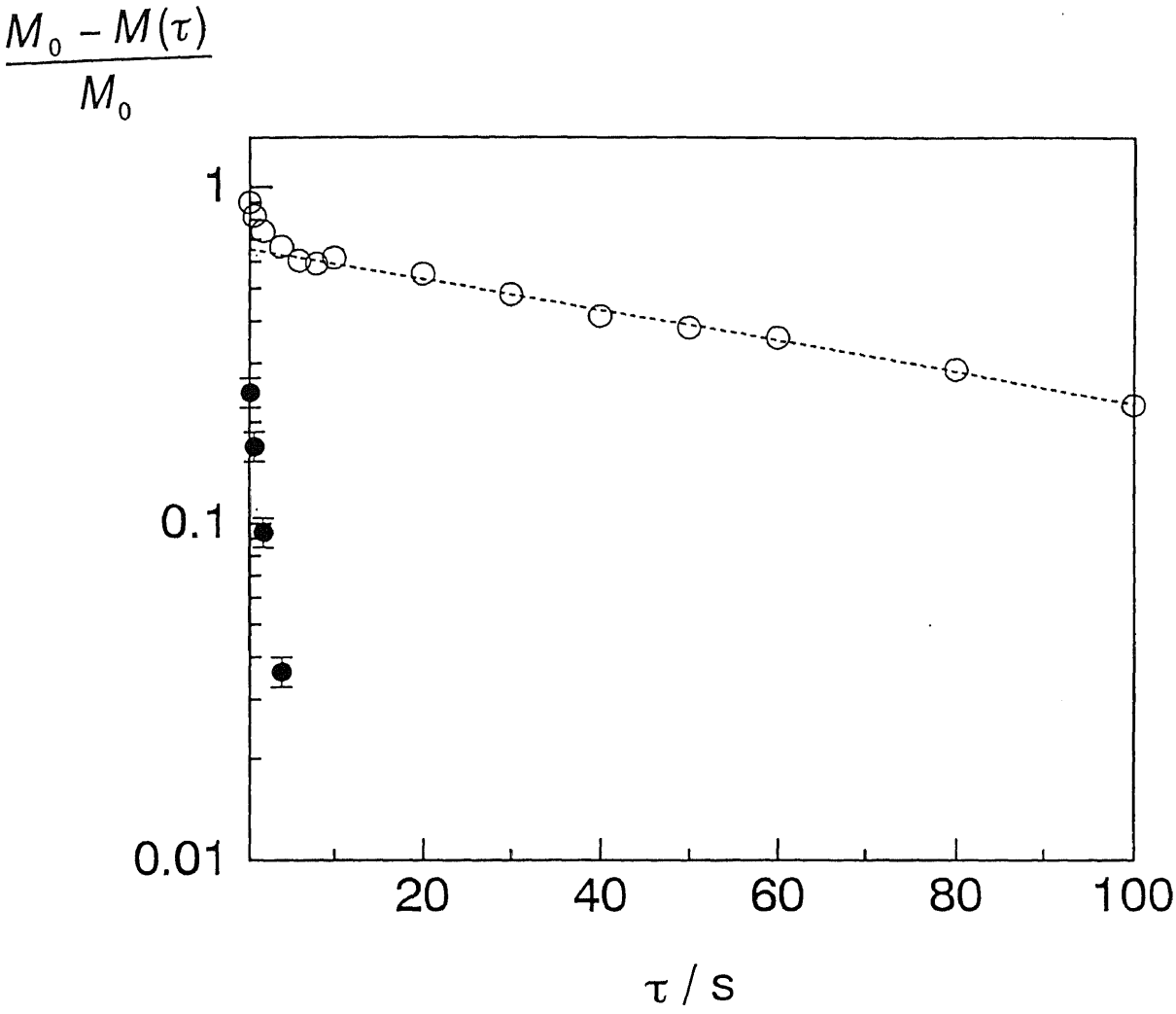

Fig. 3-5 The recovery of ^{31}P magnetization [$(M_0\text{-}M(\tau)) / M_0$] (○) after a $\pi/2$ pulse observed for the peak at 19 ppm in $(NH_4)_4[Pt_2I(P_2O_5H_2)_4]$ at room temperature (Larmor frequency: 121.496 MHz). The slope of dotted line affords a long T_1 (96 s). The fast magnetization component (●) which leads to the short T_1 is given by difference between the observed magnetization and the dotted line.

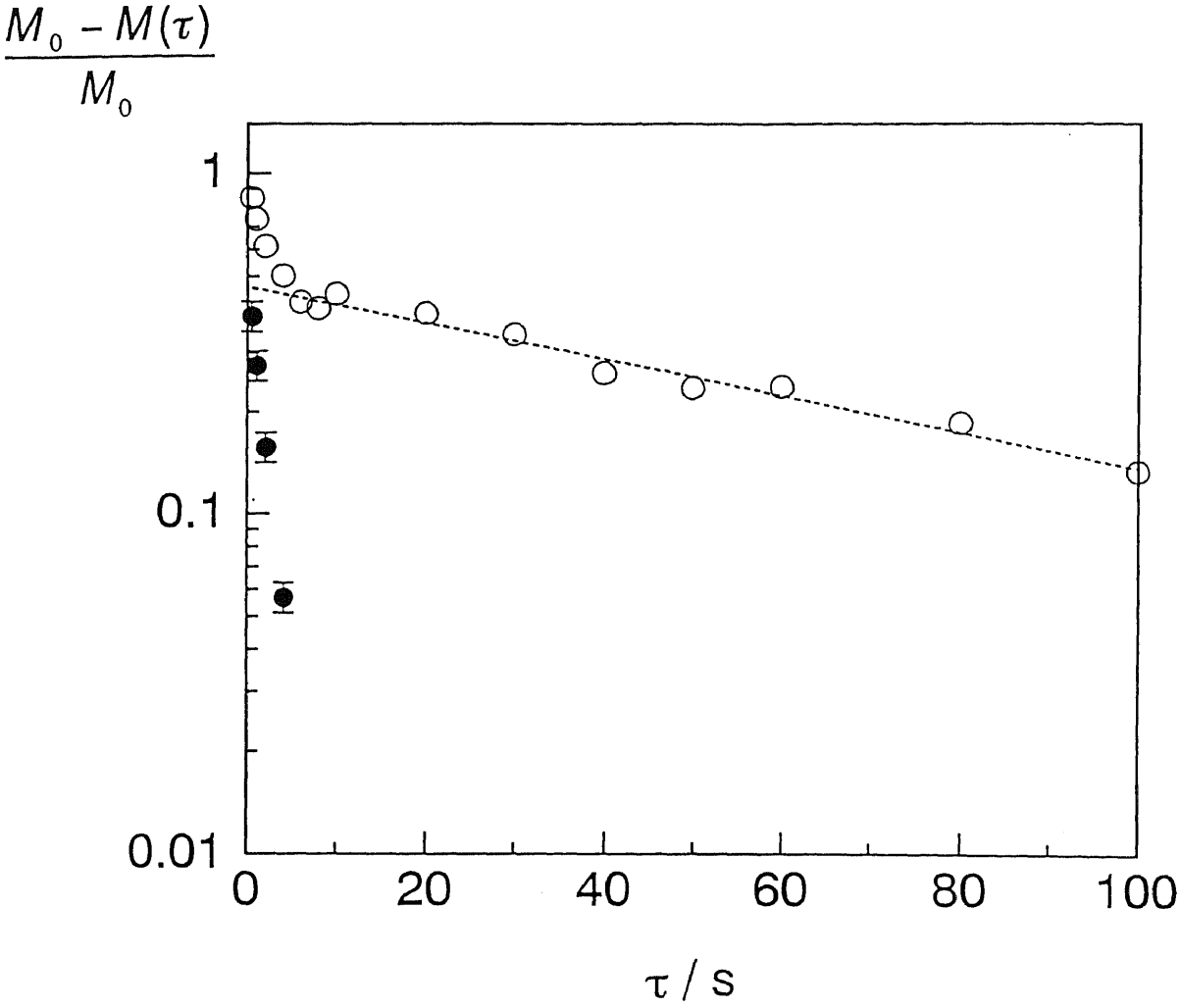

Fig. 3-6 The recovery of ^{31}P magnetization [$(M_0\text{-}M(\tau)) / M_0$] (○) after a $\pi/2$ pulse observed for the peak at 65 ppm in $(NH_4)_4[Pt_2I(P_2O_5H_2)_4]$ at room temperature (121.496 MHz). The slope of dotted line affords a long T_1 (81 s). The fast magnetization component (●) is given by difference between the observed magnetization and the dotted line.

paramagnetic sites in the crystals. These spins seem to be at impurities or the end of polymer chains.

3.4 Conclusion

^{31}P MAS NMR spectra of -Pt-Pt-X-Pt-Pt-X- type 1-D metal complexes $(NH_4)_4[Pt_2(P_2O_5H_2)_4]$ (X: Cl, Br, I) were measured at room temperature. Two kinds of resonance lines were observed in these complexes at chemical shifts of 20- 40 and 50- 70 ppm, whose values are close to those in binuclear Pt^{2+} and Pt^{3+} complexes containing $[Pt_2(P_2O_5H_2)_4]^{4-}$ and $[Pt_2X_2(P_2O_5H_2)_4]^{4-}$ ions, respectively. This result supports the mixed-valence structure model in which the valences are almost the same as Pt^{2+} and Pt^{3+} found in the monomer complexes. Since the fact that quite long ^{31}P T_1 values were observed on these complexes implies no paramagnetic spin structure, it is concluded that the valence structure is $-Pt^{2+}-Pt^{2+}-X-Pt^{3+}-Pt^{3+}-X-$.

References to Chapter 3

1. C.-M. Che, F.H. Herbstein, W.P. Schaefer, R.E. Marsh and H.B. Gray, *J. Am. Chem. Soc.*, **105**, 4604 (1983).
2. R.J.H. Clark, M. Kurmoo, H.M. Dawes and M.B. Hursthouse, *Inorg. Chem.*, **25**, 409 (1986).
3. L.G. Butler, M.H. Zietlow, C.-M. Che, W.P. Schaefer, S. Sridhar, P.J. Grunthaner, B.I. Swanson, R.J.H. Clark and H.B. Gray, *J. Am. Chem. Soc.*, **110**, 1155 (1988).
4. S. Jin, T. Ito, K. Toriumi and M. Yamashita, *Acta Crystallogr.*, **C45**, 1415 (1989).
5. M. Yamashita and K. Toriumi, *Inorg. Chim. Acta*, **178**, 143 (1990).
6. Y. Hamaue, R. Aoki, M. Yamashita and S. Kida, *Inorg. Chim. Acta*, **54**, L13 (1981).
7. M. Kurmoo and R.J.H. Clark, *Inorg. Chem.*, **24**, 4420 (1985).
8. C.-M. Che, L.G. Butler and H.B. Gray, *J. Am. Chem. Soc.*, **103**, 7796 (1981).
9. C.-M. Che, L.G. Butler, P.J. Grunthaner and H.B. Gray, *Inorg. Chem.*, **24**, 4662 (1985).
10. C.-M. Che, W.P. Shaefer, H.B. Gray, M.K. Dickson, P.B. Stein and D.M. Roundhill, *J. Am. Chem. Soc.*, **104**, 4253 (1982).
11. S.A. Bryan, M.K. Dickson and D.M. Roundhill, *Inorg. Chem.*, **26**, 3878 (1987).
12. N.F. Ramsey, *Phys. Rev.*, **78**, 699 (1950).

13. I.J. Coloquhoun and W.J. McFarlane, *J. Chem. Soc. Chem. Commun.*, 145 (1980).

Chapter 4

Electron Spin Dynamics in an Iodo-Bridged Binuclear Nickel Complex, $Ni_2(CH_3CS_2)_4I$

4.1 Introduction

A halogen-bridged one-dimensional (1-D) complex $Ni_2(CH_3CS_2)_4I$ has the -M-M-X-M-M-X- type structure similar to that of $(NH_4)_4[Pt_2X(P_2O_5H_2)_4]$ reported in Chapter 3. This type complex is expected to have an electron structure delocalized more than in the -M-X-M-X- type because of the presence of metal-metal bonds. In fact, $Ni_2(CH_3CS_2)_4I$ has been reported to have a high electrical conductivity of 2.5×10^{-2} S cm^{-1} at room temperature [1] and a valence structure of $-Ni^{2.5+}-Ni^{2.5+}-I-Ni^{2.5+}-Ni^{2.5+}-I-$ with no Peierls distortion was predicted from the measurements of X-ray diffraction [1,2] and magnetic susceptibility [1]. The dimeric unit contains four bridging dithioacetato ligands, and each nickel atom is surrounded by four sulfur atoms forming a square planar arrangement as shown in Fig. 4-1. In the present chapter, the electron spin dynamics in $Ni_2(CH_3CS_2)_4I$ is discussed in detail from the analysis of the solid-state ^{13}C CP / MAS NMR spectra and ^1H NMR relaxation measurements.

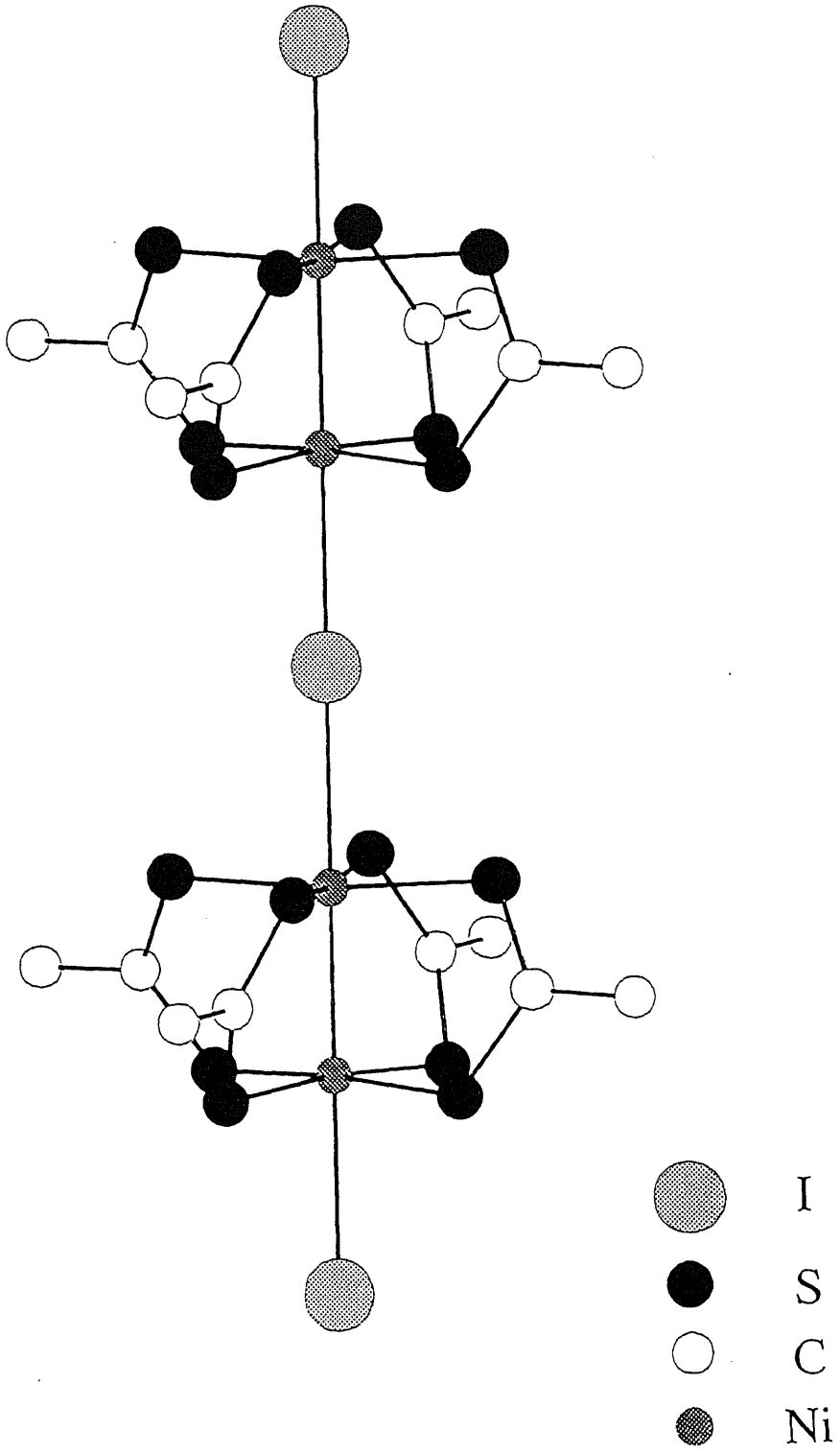

Fig. 4-1 The structure of the iodo-bridged one-dimensional (1-D) complex, $Ni_2(CH_3CS_2)_4I$ determined by X-ray diffraction at room temperature [1,2].

4.2 Experimental

NMR measurements were performed on the crystals prepared by the reported method [2]. ^{13}C CP / MAS NMR spectra were measured with a Bruker MSL-300 spectrometer at Larmor frequencies of 75.468 and 300.13 MHz for ^{13}C and ^{1}H, respectively, at room temperature. The contact time was chosen to be 1.0 ms and the spectra were accumulated 15,000 scans with a repetition time of 10 s. The chemical shift of glycine carbonyl carbon at 176 ppm was used as the external standard.

Temperature and Larmor frequency dependences of ^{1}H NMR spin-lattice relaxation time T_1 were measured in ranges of 90- 300 K and 20- 300 MHz using a home-made pulsed spectrometer reported in Chapter 2 and a Bruker MSL-300 spectrometer. The inversion recovery method applying the π- t- $\pi/2$ pulse sequence where t is the time interval between π and $\pi/2$ pulses was employed to determine T_1.

4.3 Results and Discussion

4.3.1 ^{13}C CP / MAS NMR Spectra

The observed ^{13}C CP / MAS NMR spectrum of a 1-D polymer complex $Ni_2(CH_3CS_2)_4I$ at room temperature is shown in Fig. 4-2. The sharp doublet lines ($\delta \approx$ 30 ppm) could be assigned to two kinds of nonequivalent CH_3 groups in crystal. The widths of these spectra were broader than those observed in the Ni^{2+} monomer complex $Ni_2(CH_3CS_2)_4$ as shown in Fig. 4-3. We can see another line from Fig. 4-2 which is accompanied by several side bands spread out over 200- 300 ppm was observed at *ca.* 250 ppm. This broad signal assignable to the CS_2 group implies that fluctuation of the electron spins on the $-Ni^{2.5+}-Ni^{2.5+}-I-$ chain influences the ^{13}C NMR signal. To investigate the dynamic behaviour of these spins in $Ni_2(CH_3CS_2)_4I$ more in detail, ^1H NMR spin-lattice relaxation time T_1 was measured.

4.3.2 ^1H NMR Spin-Lattice Relaxation Time T_1

The observed ^1H magnetization recovery after the inversion recovery pulse sequence showed marked non-exponential behaviour in the whole temperature (90- 300 K) and frequency (20- 300 MHz) ranges investigated. An observed recovery curve shown in Fig. 4-4 can roughly be expressed as the superposition of two definite T_1 components, T_{1S} and T_{1L}, each of which could be given by

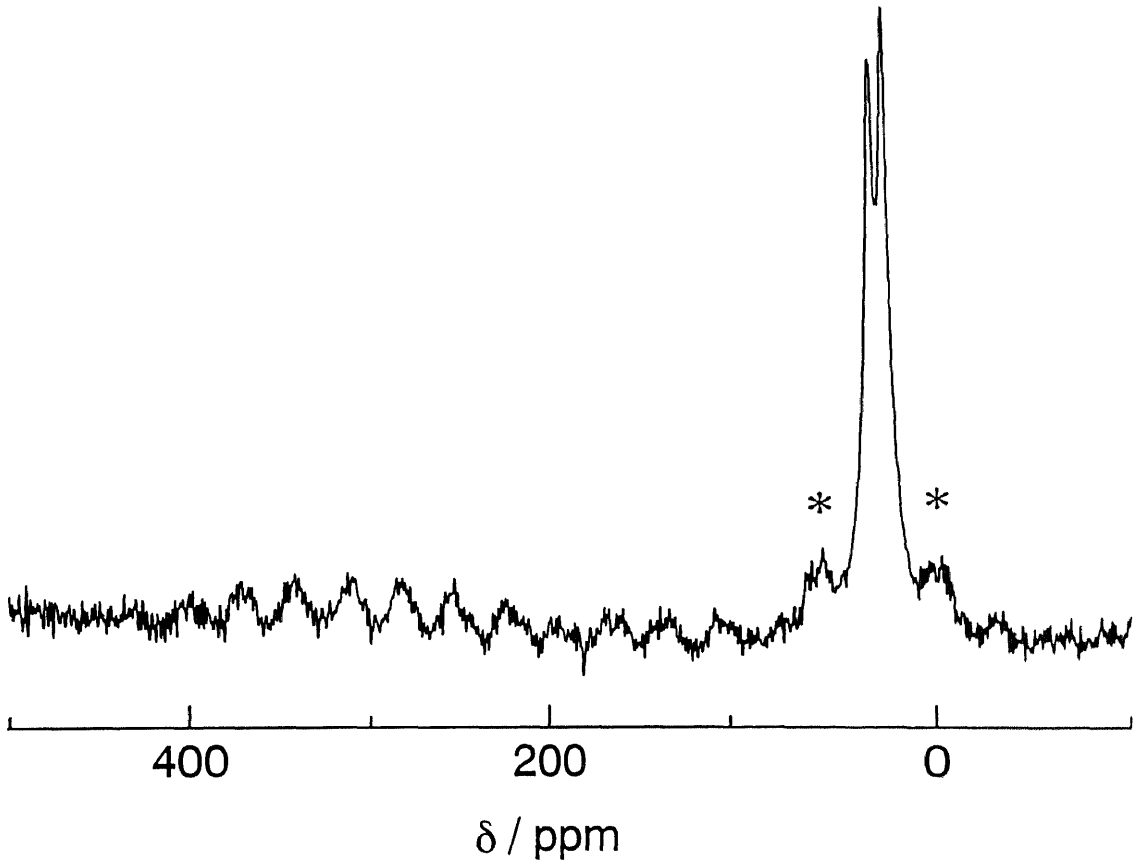

Fig. 4-2 A ^{13}C CP / MAS NMR spectrum of the 1-D polymer complex, $Ni_2(CH_3CS_2)_4I$ observed at room temperature. Asterisks are spinning sidebands of the sharp doublet line. A spinning rate of *ca.* 2.2 kHz was employed.

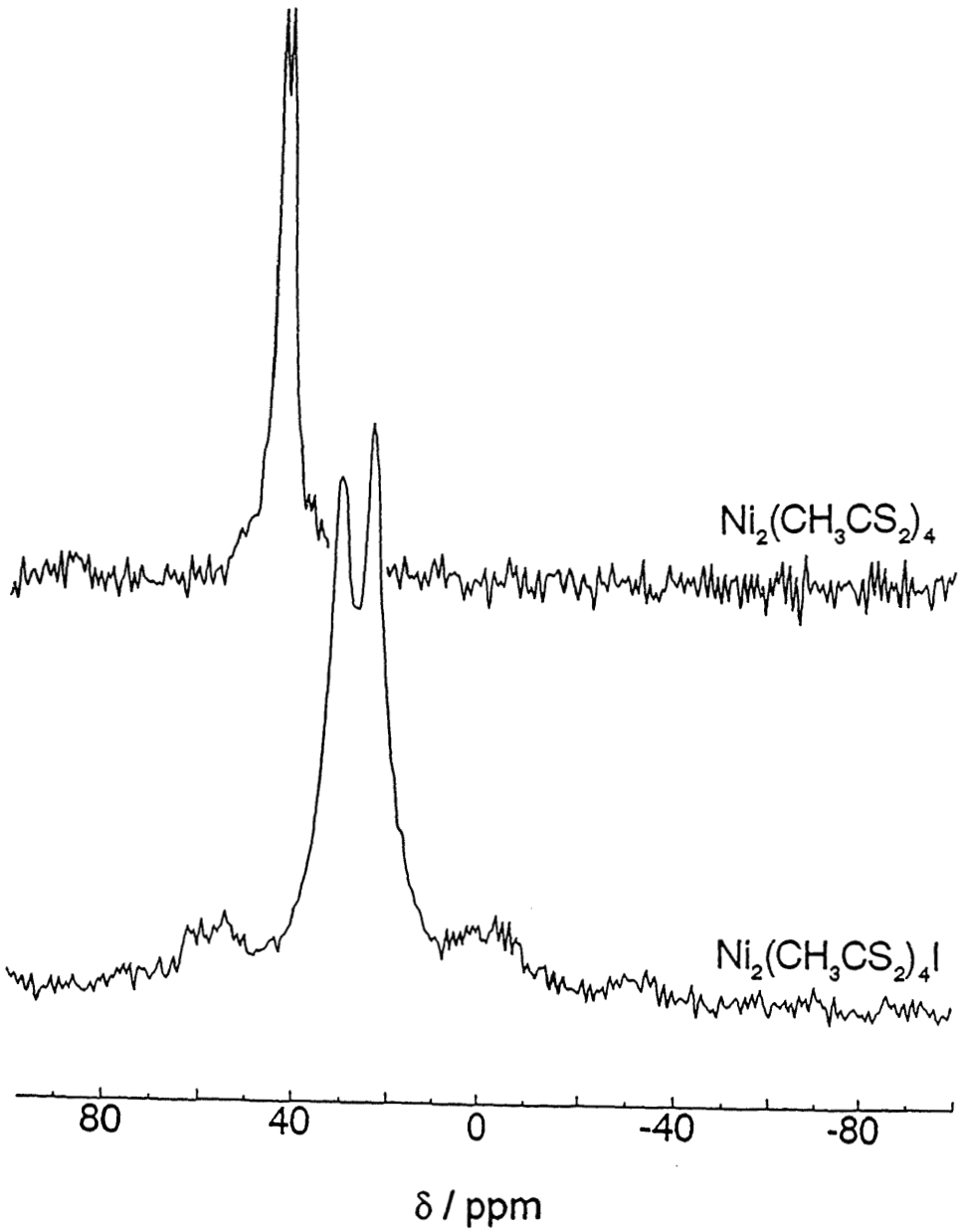

Fig. 4-3 ^{13}C CP / MAS NMR spectra of the monomer Ni^{2+} complex $Ni_2(CH_3CS_2)_4$ and the polymer $Ni_2(CH_3CS_2)_4I$ observed at room temperature.

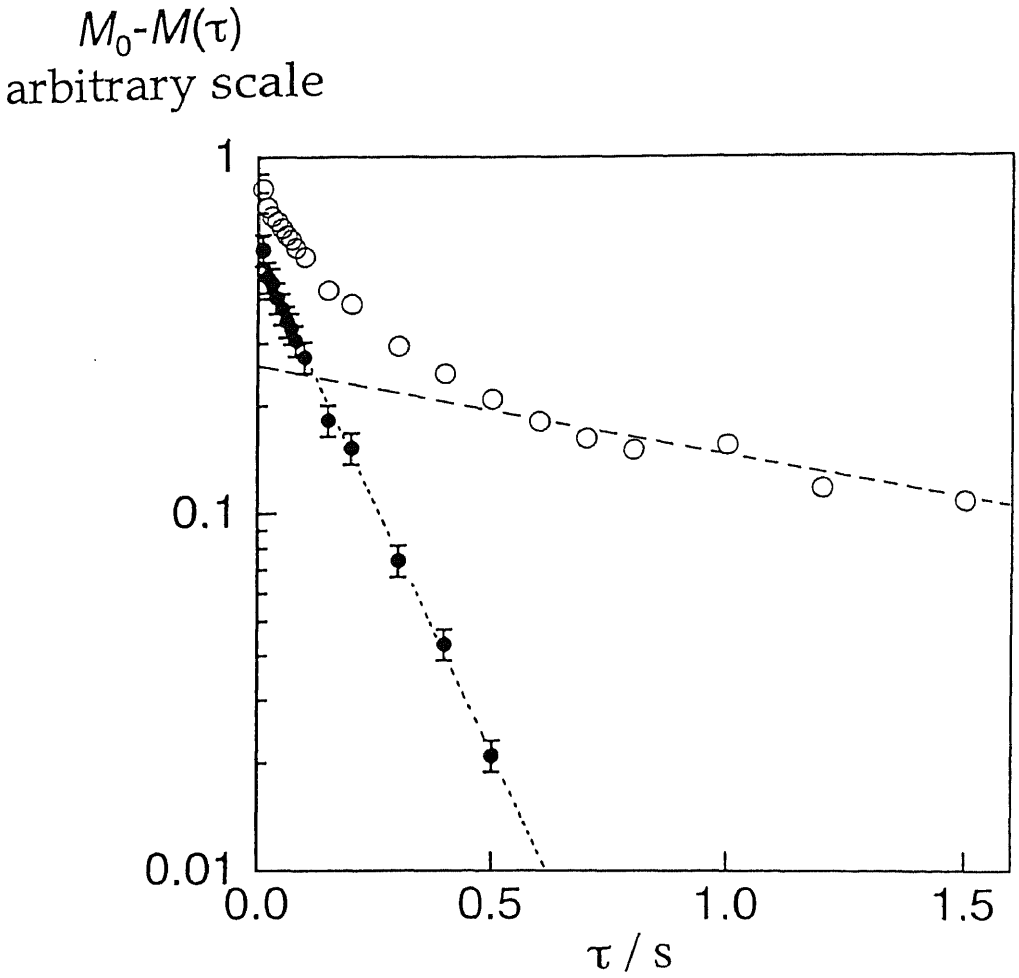

Fig. 4-4 Recovery of ^{1}H magnetization, [M_0- $M(\tau)$] (○) observed after a $\pi/2$ pulse at 291 K (34.80 MHz). The slope of the broken line affords the long T_{1L}=1.45 s. The magnetization of the short T_{1S} component (●) is given by the difference between the observed magnetization and the broken line. The slope of the dotted line gives T_{1S}= 0.15 s.

$$M(\tau) = M_0[1-2\exp(-\frac{\tau}{T_1})], \qquad (4\text{-}1)$$

where M_0 and $M(\tau)$ are ^{1}H magnetizations after π- t- $\pi/2$ pulses observed in the limit of $t \rightarrow \infty$ and $t = \tau$, respectively as discussed in Chapter 2. The shorter T_{1S} was always the major component (*ca. 65 %*) and the ratio of its magnetization to the long T_{1L} component was almost independent of temperature as shown in Fig. 4-5. In the present analysis, the major magnetization component giving T_{1S} is employed. The temperature dependences of the T_{1S} observed at 21.07 and 40.98 MHz are shown in Fig. 4-6. The T_{1S} gave almost temperature independent values with a slight increase with temperature. This temperature independency could be explained by the relaxation due to electron spin flips between the neighbouring -$Ni^{2.5+}$-$Ni^{2.5+}$-I- units [3,4]. The long T_{1S} of the order of 0.1 s observed at 40.98 MHz suggests a strong interaction between the spins in consistent with the model of the antiferromagnetically strongly coupled 1-D spin structure proposed from the analysis of the magnetic susceptibility data [1].

In the temperature range studied, the observed frequency (ω_H) dependence of T_{1S} gave a linear relation between T_{1S}^{-1} and $\omega_H^{-1/2}$ as shown in Fig. 4-7 where the data at three typical temperatures, 146, 178 and 291 K are shown. Applying the Devreux's treatment [5,6] on the 1-D spin-dynamics as given in Chapter 2, T_1 is given by

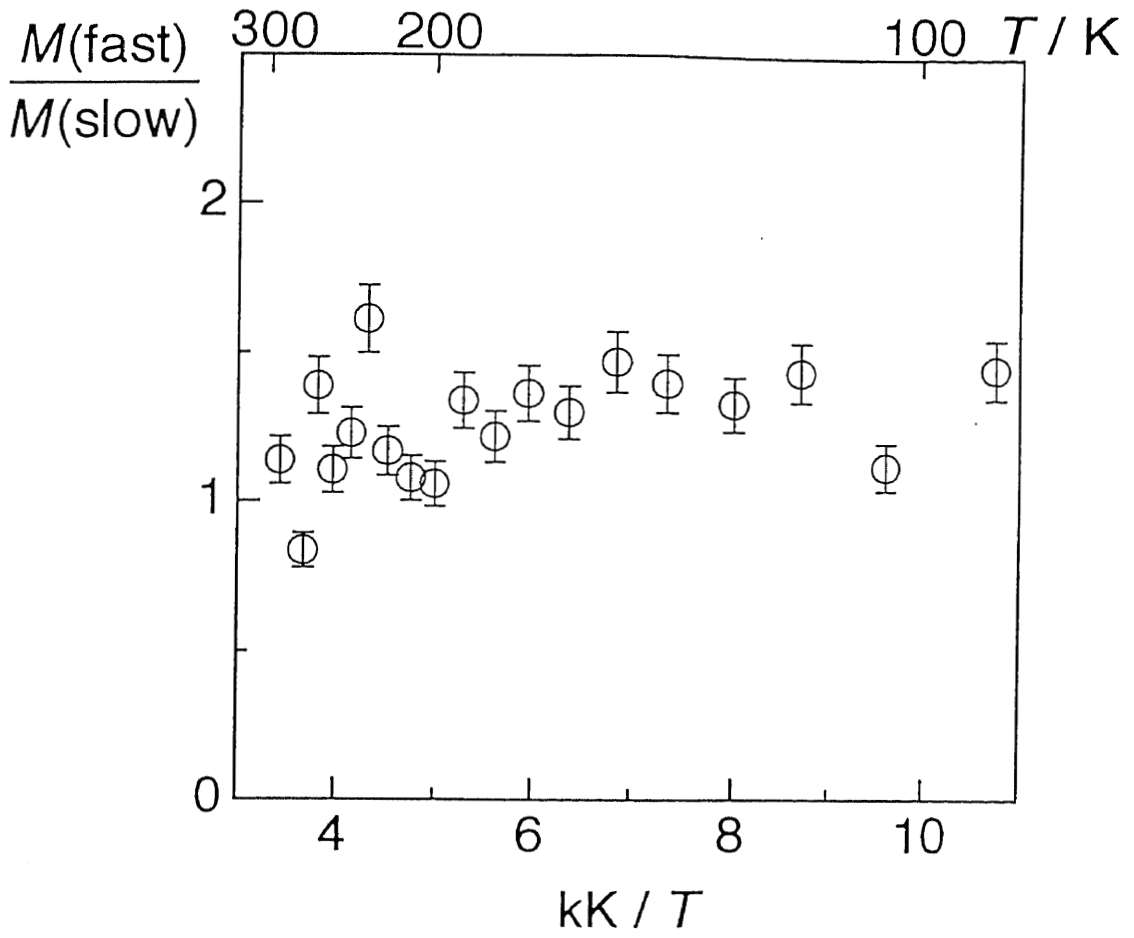

Fig. 4-5 A temperature dependence of the magnetization ratio, [M(fast) / M(slow)] of the fast to the slow recovering component observed at 40.98 MHz.

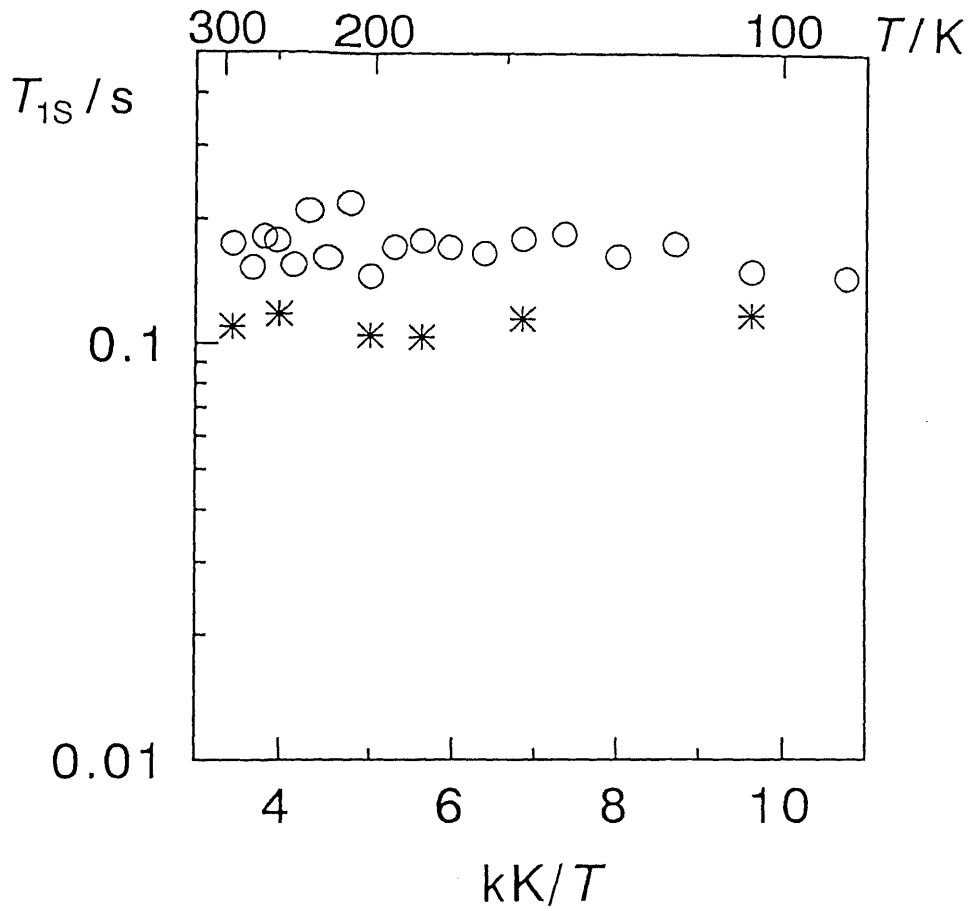

Fig.4-6 Temperature dependences of ^{1}H T_{1S} (short component) observed at Larmor frequencies of 21.07 (*) and 40.98 MHz (○).

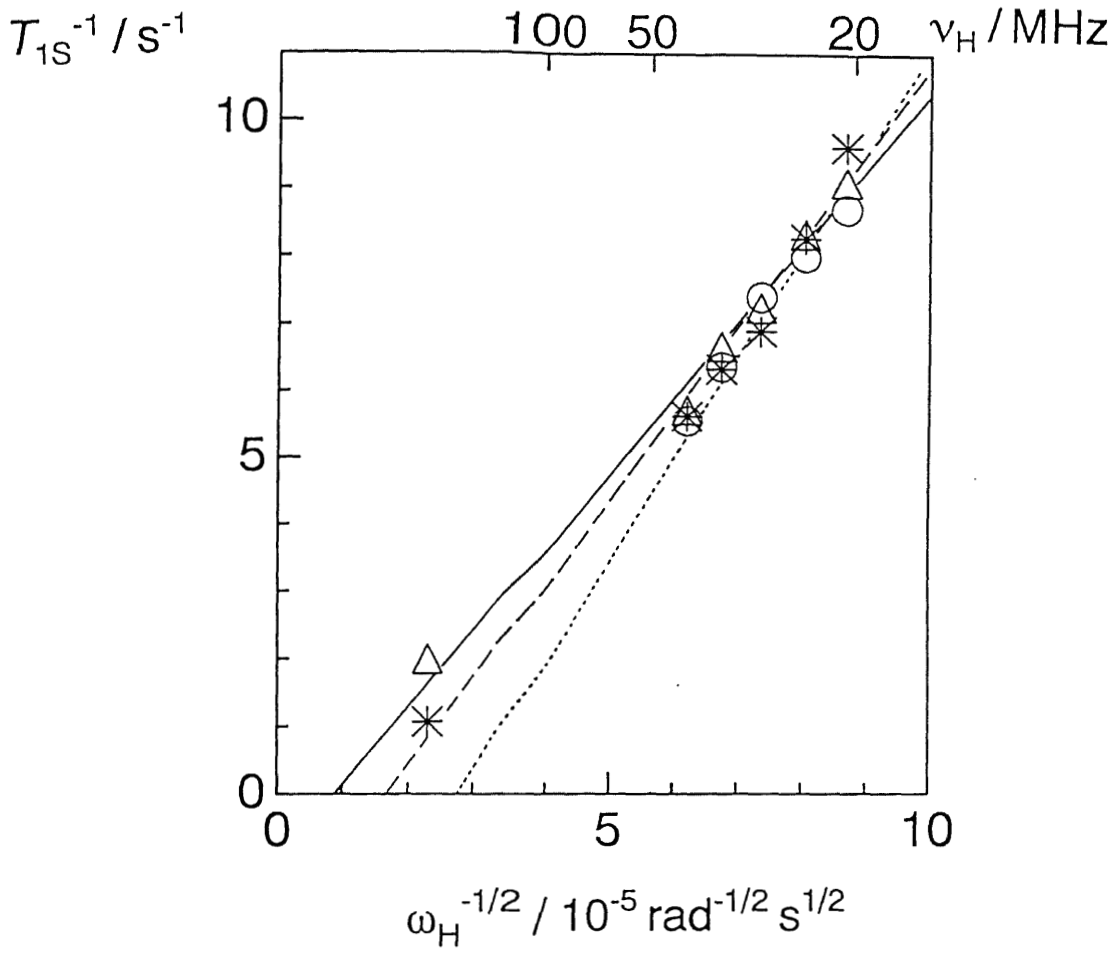

Fig.4-7 Larmor frequency dependences of ^{1}H T_{1S}^{-1} (short component) plotted against $\omega^{-1/2}$ at 146 (○), 178 (*) and 291 K (△). The 1-D electron spin diffusion rate D^* and delocalization length λ are obtained from the slope and the intercept with the $\omega^{-1/2}$ axis in the dotted (146 K), broken (178 K) and solid lines (291 K).

$$T_1^{-1} = kT\chi_s \frac{d^2}{5}[(3+7\sqrt{\frac{\gamma_H}{\gamma_e}})(2D^*\omega_H)^{-\frac{1}{2}} - \frac{5C}{D^*}], \quad (4\text{-}2)$$

where χ_s, d and C denote the electron spin susceptibility, the magnetic dipolar coupling constant between the protons and electrons and a constant expressed as

$$C=2\gamma\lambda \quad (4\text{-}3)$$

with γ= 0.33 for λ>5, respectively. The diffusion rate D^* and the spin delocalization length λ for 1-D hopping of electron spins were evaluated from the slope of the plots and the intercept with the $\omega_H^{-1/2}$ axis in the observed T_{1S}^{-1} versus $\omega_H^{-1/2}$ plots. In this calculation, we used χ_s= 2.9×10^{12} emu erg^{-1} cm^{-3} and d= 1.66×10^{13} rad^4 s^{-2} which were roughly estimated from the magnetic susceptibility data [1] and the crystal structure [1,2], respectively. Using these values, D^* and λ were calculated respectively to be 8.4×10^{12} rad s^{-1} and 57 at 146 K, 1.8×10^{13} rad s^{-1} and 52 at 178 K, and 6.2×10^{13} rad s^{-1} and 47 at 291 K. The temperature dependence of D^* in the range between 100 and 300 K could be determined as shown in Fig. 4-8. Large D^* values of the order of 10^{13} rad s^{-1} obtained implies rapid 1-D spin migration with a low activation energy of 48±5 meV (= 4.8±5 kJ mol^{-1}) below *ca.* 140 K. The spin delocalization length of *ca.* 50 units was evaluated, and this length is much longer than *ca.* 20 units evaluated for the

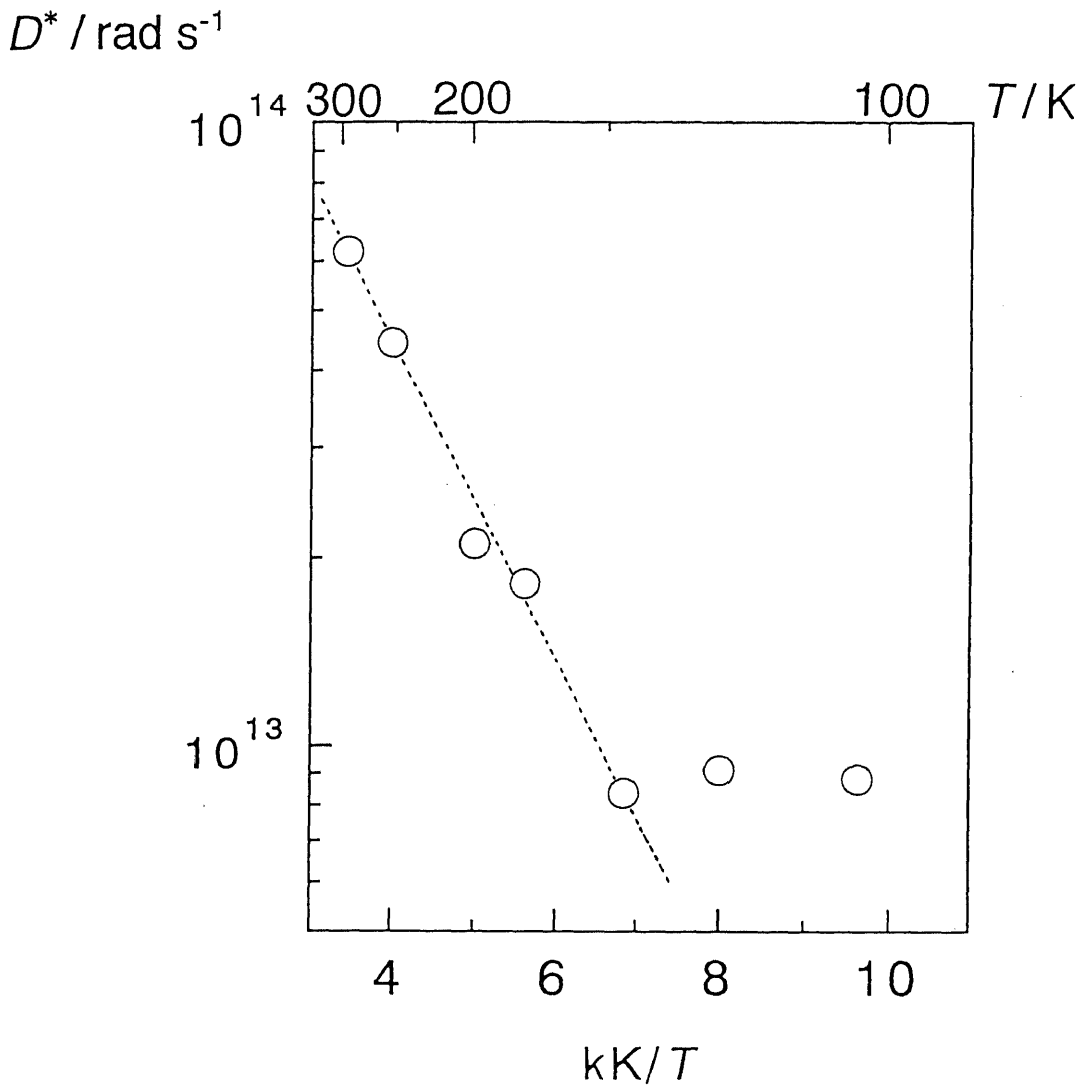

Fig.4-8 The temperature dependence of 1-D diffusion rate D^* of electron spins. The slope of the dotted line gives the activation energy of 48 ± 5 meV.

$[Pd(chxn)_2][PdBr_2(chxn)_2]Br_4$ [7] and $[Pd(en)_2][PdBr_2(en)_2](ClO_4)_4$ (see Section 2.3.2) which have a $-Pd^{2+}-Br-Pd^{4+}-Br-$ type valence structure with the Peierls distortion.

4.4 Conclusion

^{13}C CP / MAS NMR spectra observed at room temperature and ^{1}H NMR relaxation in the range of 90- 300 K measured on $Ni_2(CH_3CS_2)_4I$ showed marked influence from paramagnetic spins on 1-D -$Ni^{2.5+}$-$Ni^{2.5+}$-I- chain. The almost temperature independent long T_1 of *ca.* 0.1 s is attributable to the relaxation due to the fluctuation of antiferromagnetically coupled unpaired electron spins formed in the - Ni - Ni - I - chain. T_1^{-1} in this temperature range was shown to have a linear relation with $\omega^{1/2}$ which was explained well by the model of rapid spin diffusion along the 1-D chain. Applying the Devreux's treatment on the 1-D spin dynamics, the diffusion rate, activation energy for the 1-D hopping of electron spins and the spin delocalization length were evaluated to be the order of 10^{13} rad s^{-1}, 48 ± 5 meV and *ca.* 50 units, respectively.

References to Chapter 4

1. M. Yamashita, Y. Wada, K. Toriumi and T. Mitani, *Mol. Cryst. Liq. Cryst.*, **216,** 207 (1992).

2. C. Bellitto, G. Dessy and V. Fares, *Inorg. Chem.*, **24**, 2815 (1985).

3. H. Rager, *Z. Naturforsch.*, **36a**, 637 (1981).

4. A. Birkeland and I. Svare, *Phys. Scr.*, **18**, 154 (1978).

5. F. Devreux, J.-P. Boucher and M. Nechtschein, *J. Phys.* (Paris), **35**, 271 (1974).

6. F. Devreux, *Phys. Rev.*, **B25**, 6609 (1982).

7. R. Ikeda, M. Iida, T. Asaji, A. Ghosh and M. Yamashita, *Chem. Phys. Lett.*, **210**, 78 (1993).

Acknowledgements

The encouragement and support of Dr. Ryuichi Ikeda, Professor of University of Tsukuba, is greatly appreciated.

The author wishes to thank Drs. Hiroshi Ohki in Hiroshima University and Shin'ichi Ishimaru in University of Tsukuba for many helpful discussions and suggestions.

Grateful acknowledgement is made to Dr. Masahiro Yamashita and the members of his group in Nagoya University for helpful advice on the preparation and providing samples.

Sincere thanks are for Dr. Izumi Nakai and the members of his group for their kindness to allow me to use the powder X-ray diffractometer. The author also expresses his thanks to Chemical Analysis Center, University of Tsukuba, for the measurement of elemental analysis.

Thanks are given to Drs. Noriko Yamamuro, Subratanath Konor, and Ashutosh Ghosh and Messrs. Yukitaka Nakano, Hidenori Suzuki, and Toru Hachisuka for their assistance in the experimental work.

It remains for me to thank Drs. Hitoshi Shoji, Riki Seki, Isoroku Nagasawa, and Yukihiro Yokoyama and all my colleagues for their support and assistance.